ADVANCED ENERGY MATERIALS
www.advenergymat.de

Stress Relief in Metal Anodes: Mechanisms and Applications

Jianan Gu, Yu Shi, Zhiguo Du, Meicheng Li,* and Shubin Yang**

Metal anodes (lithium/sodium/zinc) are recognized as the most promising choice for rechargeable batteries due to their high theoretical capacity and low electrochemical redox potential. Unfortunately, metal anodes face serious metal dendrite problems, hindering their practical applications. Recent research has shown that metal dendrites can also be caused by high levels of stress generated during the metal deposition process. To address this issue, an alternative strategy based on stress relief is proposed to inhibit the growth of metal dendrites. Herein, this work aims to investigate the mechanism of stress generation and evolution within metal anodes. In addition, this work explores the utilization of stress to induce metal nucleation. This work further discuss the various experimental techniques used to study stress release in metal dendrites and review recent research findings on stress relief in metal dendrites within metal anodes. Specifically, this work examines how microstructure and processing conditions affect stress release and discuss potential strategies for improving the efficiency of stress relief strategies in metal dendrites. As a result, a deeper understanding of stress release in metal dendrites can lead to the development of rechargeable batteries with superior performance, longer cycle life, as well as enhanced safety for practical applications in various fields.

1. Introduction

Rechargeable batteries with metal anodes (lithium, sodium, and zinc), are considered as the most promising candidates for the future electric vehicle, large-scale electric grids, and energy storage devices.[1–6] Metal anodes not only possess high theoretical capacity but also have relatively low electrochemical potential.[7–13] For instance, metallic Li anode has a high theoretical capacity up to 3860 mAh g^{-1} and a low electrochemical potential of −3.04 V (versus standard hydrogen electrode).[14–20] However, during repeated charge–discharge process, metal anodes are prone to generate metal dendrites on their surface of electrode.[21–27] Metal dendrites tend to grow during the plating process and can penetrate the separator, causing short circuits within the battery. Besides, metal dendrites can cause active material loss from the anode, reducing the overall capacity of the battery. Additionally, the growth and dissolution of dendrites during cycling can lead to cycling instability, resulting in capacity fade and reduced cycle life.[28–32]

To address the metal dendrite issue, researchers direct their attention to the process of dendrite generation. This process mainly involves the nucleation and growth stages, as delineated by the Sand's time model.[23,33,34] Thus, various strategies based on this have been adopted, including 3D host structure,[35–45] artificial solid electrolyte interphase (SEI) film,[46–54] and controlled nucleation.[55–64] For instance, conductive materials like copper (Cu) or nickel have been utilized to create a sponge-like structure as a 3D host to restrain the growth of metal dendrite.[65,66] The 3D porous structure efficiently redistributes the electric field and decreases the current density as well as provides a large surface area for metal deposition, reducing the nucleation overpotential and suppressing dendrite growth. Additionally, both organic and inorganic materials have been used to create artificial SEI films that build a protective sheath on the electrode's surface and inhibit the growth of dendrite.[67] Organic materials like polyethylene oxide,[68] poly(acrylic acid),[69–71] and poly(vinylidene fluoride)[72] provide a flexible and conformal coating, while inorganic-based SEI films like lithium phosphate,[73] lithium borate,[74,75] or lithium fluoride[72,76–78] provide better mechanical and chemical stability. Controlled nucleation strategy is a highly effective strategy for preventing the formation of dendrite at initial stage during metal deposition process. For instance, Prof. Cui and his co-workers have developed a unique nanocapsule structure for Li deposition that incorporates hollow carbon spheres with nanoparticle seeds inside.[79] When used for Li deposition substrate, they found that lithium metal primarily grew inside the hollow carbon spheres and resulted in uniform Li plating on the surface of electrode. This method effectively eliminates dendrite formation and enables the anode to

J. Gu, M. Li
State Key Laboratory of Alternate Electrical Power System with Renewable Energy Sources, School of New Energy
North China Electric Power University
Beijing 100096, China
E-mail: mcli@ncepu.edu.cn
Y. Shi, Z. Du, S. Yang
School of Materials Science and Engineering
Beihang University
Beijing 100191, China
E-mail: duzhiguo@buaa.edu.cn; yangshubin@buaa.edu.cn
The ORCID identification number(s) for the author(s) of this article can be found under https://doi.org/10.1002/aenm.202302091

DOI: 10.1002/aenm.202302091

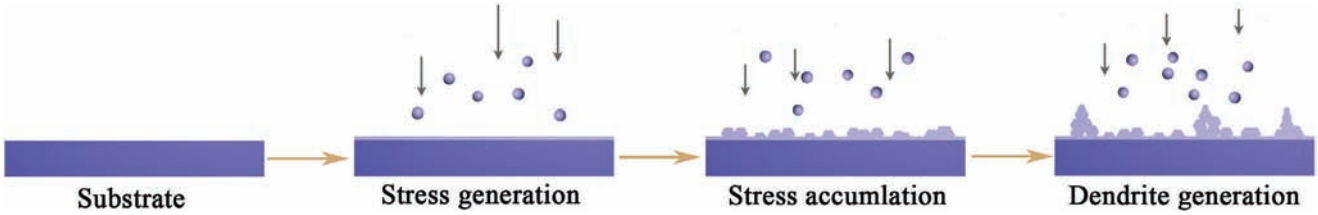

Figure 1. Schematic illustration of metallic dendrite generation caused by continuous dendrite generation and accumulation.

exhibit improved cycling performance, even when exposed to corrosive alkyl carbonate electrolytes. Moreover, the as-resulted Li anode maintains a high Coulombic efficiency (CE) for over 300 cycles, demonstrating the effectiveness by using this innovative approach.[79] Although the above three strategies have effectively suppressed the metal dendrites at a certain point, these strategies ignored the critical influence of the stress generated in the metal plating process (**Figure 1**).

Stress is a ubiquitous phenomenon in the realm of thin film deposition, also including the metal electrochemical deposition.[80] The impact of stress on the functionality, dependability, and robustness of material components cannot be overstated, particularly in the behavior, characteristics, and properties of thin films, where it can result in a range of issues, including cracking, peeling, buckling, and blistering. Recent studies show that metal dendrites can originate from the stress generated at the surface of electrodes during metal deposition process.[81–83] As a result, an alternative methodology by releasing stress strategy has been adopted to eliminate the formation of metal dendrite, increasing the CE as well as cyclic stability of metal anodes.[84,85] Stress relief in metal dendrites is a critical aspect to be considered in improving the property as well as safety of batteries with metal anodes. Although the mechanism of stress generation and accumulation in metal dendrites has been extensively studied,[86–92] understanding the factors that influence stress relief in metal dendrites, such as microstructure and processing conditions, is crucial for developing effective strategies to mitigate the formation of metal dendrite (**Figure 2**).

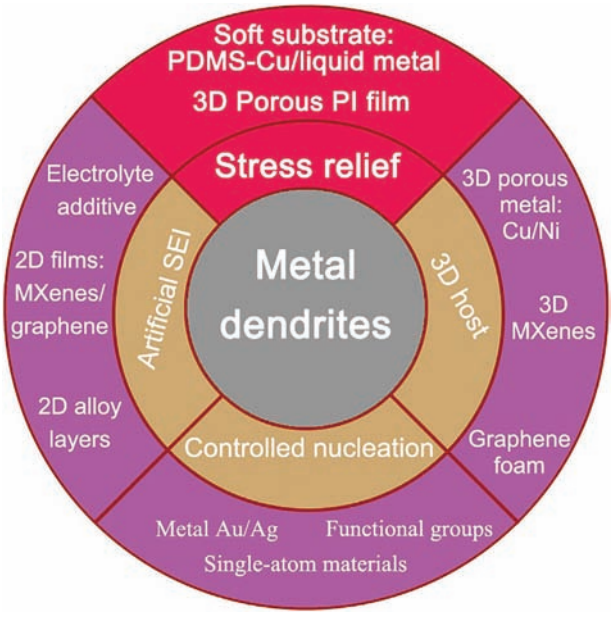

Figure 2. Schematic illustration of main strategies for solving metal dendrite issues.

Herein, we aim to explore the mechanism of stress generation and evolution during the metal deposition process. Besides, the utilization of stress to induce metal nucleation in metal anodes was further discussed. Besides, we discuss the various experimental techniques used to study stress release in metal dendrites and review recent research findings on stress relief in metal dendrites of metal anodes such as Li and Zn. Specifically, we examine how microstructure and processing conditions affect stress relief strategy and discuss potential strategies for improving the efficiency of stress relief strategy in metal dendrites. Ultimately, a deeper understanding of stress relief in metal dendrites can lead to the creation of rechargeable batteries with improved properties, longer cycle life, as well as enhanced safety for practical applications in various fields (**Figure 3**).

2. Stress Generation and Evolution Mechanism in Metal Deposition Process

2.1. Stress Generation and Evolution in Metal Deposition Film

The stress in metal deposition is influenced by several kinetic processes, such as deposition, diffusion, and microstructure evolution. Deposition process, including nonenergetic processes like evaporation or electrodeposition, can result in atoms with low kinetic energy.[93,94] As for the nonenergetic processes, the stress-thickness relationship of a deposition film depends on various factors, including material type, atomic mobility, temperature, as well as growth rate. Stress behavior can be categorized as type I and type II.[95] In deposition films with Type I stress behavior, the tensile stress remains constant or even increases with increasing film thickness, but the stress does not relax when growth is interrupted. Conversely, in Type II stress, the film exhibits a transition from tensile to compressive stress with increasing thickness and relaxation upon interruption of growth. Grain size also affects stress evolution, and stress may relax during film growth interruption.[96,97] Recent developments in rate-equation-based models have significantly enhanced our understanding of how stress is related to temperature, growth rate, and microstructure evolution. The measurement of stress can help identify the underlying kinetic processes that govern its behavior. Additionally, the onset of island coalescence with the increase of tensile stress suggests that the formation of grain boundaries may have an impact. Hoffman proposed a mechanism that took into account the energy required to create grain boundaries between islands and elastic deformation of the islands.[98] The maximum

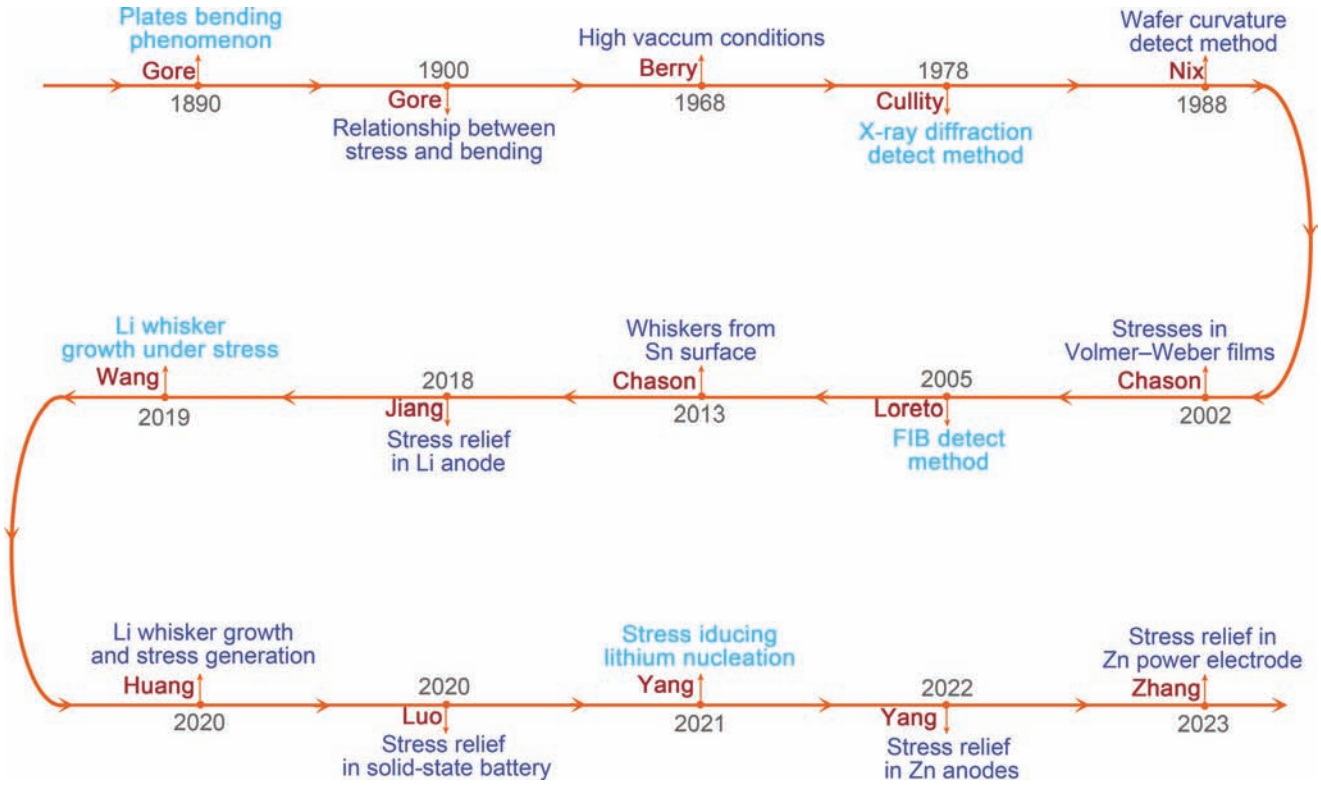

Figure 3. Timeline of the development of stress generation in thin films and stress relief strategy using in metallic anodes.

tensile stress, can be determined by the formula: $\sigma_T = 2(\frac{M_f \triangle_\gamma}{L})^{\frac{1}{2}}$ (M_f: the film's biaxial modulus, $\triangle_\gamma$: the change in interfacial energy, and L: the grain size). If the interfacial energy decreases more than the increase in strain energy, neighboring islands will coalesce and form new grain boundaries.

Regarding the energetic processes, such as magnetron sputtering for the growth of metal deposition film, energetic particle bombardment strongly influences stress, affecting both surface and subsurface processes.[99] For instance, low-mobility materials that exhibit tensile stress under non-energetic deposition conditions undergo a shift to compressive stress under energetic particles deposition. The change in stress is particularly noticeable in sputter deposition, where a broad energy distribution is generated due to the energetic particles striking the surface of the thin films, resulting in elastic deformation.

2.2. Stress Generation and Evolution in Metal Dendrite

For more than 50 years, researchers have been studying the growth of whiskers on the surface of tin (Sn), which are thin filamentous protrusions that can cause significant loss and safety issues in commercial electronics (**Figure 4**a,b). While the addition of plumbum (Pb) can prevent the formation of Sn whisker, the shift toward Pb-free manufacturing has renewed interest in understanding the complex multilayer microstructure underlying whisker growth. In particular, Prof. Chason and his co-workers have investigated the factors that drive the growth of Sn whiskers, including their direction, grain structure, and the formation of intermetallic compound (IMC).[81] They have also explored how the stress distribution in a Sn film changes after the growth of IMC, and how Sn whisker growth can relieve stress in the surrounding region. The FIB (focused ion beam) cross-sectional image in Figure 4c proved that the intricate multilayer microstructure of a Sn layer, featuring a whisker that has grown nearly parallel to the surface and displaying multiple grain orientations. At the base of the Sn whisker, a large grain extends through the entire film.[81] In contrast, the surface feature depicted in Figure 4d, possesses a low aspect ratio and spans different grains in the layer. This indicates that the formation of hillock, rather than whisker, occurs when grain boundaries are highly mobile. This could be attributed to the fact that impurity segregation to grain boundaries affects the morphology.[100]

To demonstrate the influence of grain boundary diffusion on stress evolution, elements of the model were conducted (Figure 4e,f). The model assumes a honeycomb grain structure with vertical boundaries and hemispherical particle expansion at the Sn-Cu interface. These simulations reveal that fast grain boundary diffusion reduces stress gradients and promotes a uniform stress distribution throughout the Sn layer. Conversely, stress is confined to the IMC (intermetallic compound) particle region in the absence of grain boundary diffusion. The simulations aim to comprehend how IMC growth results in stress generation in the absence of whisker formation to alleviate stress. Additional simulations indicate that Sn whisker formation can alleviate stress in the surrounding area and promote atom diffusion toward the whisker base. The growth of Sn whiskers and hillocks is dependent on the underlying grain structure,

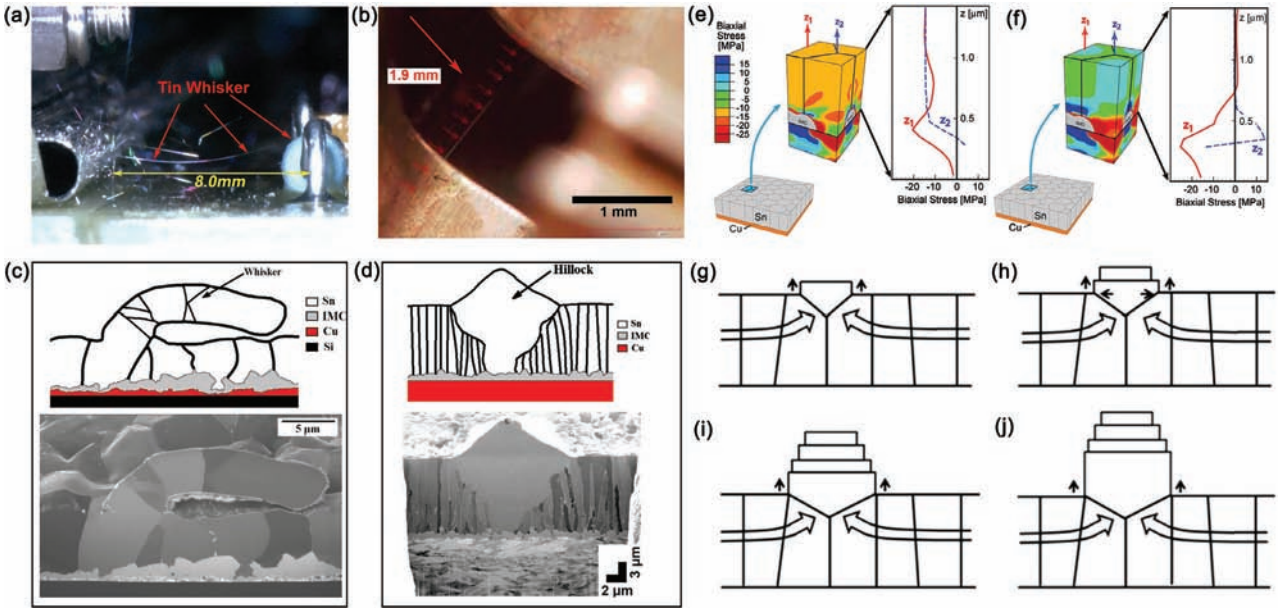

Figure 4. a) Image of whisker growing from card cage on space shuttle. b) Whisker growing across accelerator pedal position sensor from Toyota Camry. c) FIB cross-section of a whisker growing from a columnar-microstructured Sn layer electrodeposited over a fine-grain Cu layer. d) Cross-section of a hillock growing from a "'bright"' Sn layer that has been electrodeposited over Cu. e) Finite element analysis of stress distribution in Sn layer due to growth of IMC particles at interface. f) Same simulation as in part (e) but with the relaxation process of grain boundary diffusion turned off. g–j) Schematic process of the growth of a hillock, showing the alternate processes of vertical growth and grain growth, creating "wedding cake" morphology. Reproduced with permission.[81] Copyright 2013, Elsevier Ltd.

particularly the presence of "weak" grains that deform at lower stress levels than the surrounding regions. These grains are likely located at the boundaries between grains that have a horizontal component. The stress gradient created by the lower stress in the weak grain drives diffusion of mobile Sn atoms to the base of whisker/hillock, resulting in its outward growth. The rate of whisker/hillock growth is determined by the balance between the rate of IMC growth and the relaxation caused by plasticity and atom diffusion. Whiskers typically grow in a long, vertical form, while hillocks can exhibit a "wedding-cake" morphology due to sequences of vertical as well as lateral growth (Figure 4g–j).

With the fast development of characterization techniques, in situ AFM-ETEM (atomic force microscope cantilever in an environmental transmission electron microscope) has been adopted to investigate the metallic Li nucleation and growth processes with stress evolution. By using in situ AFM-ETEM technique (**Figure 5**a–c), Prof. Wang and his co-workers observed the Li nucleation and growth processes (Figure 5d,e) and demonstrated that Li growth morphology was highly impacted by ionic conductivity and mechanical stress, offering profound comprehending for Li nucleation and growth mechanism.[101] When employed mechanical stress onto Li whiskers via AFM cantilever, they found that different behaviors exhibited, including mechanical yielding, buckling, kinking, or cessation of growth (Figure 5f–n). Furthermore, a chart (Figure 5o) was presented that summarized the interplay between different interaction scenarios on a conventional chart that mapped the growth force against whisker length. This suggests that the stress thresholds for mechanical yielding and buckling correspond to the situation of Li metal with a single crystal structure, whereas the critical stress for kinking and halting deposition at the interface could substantially vary depending on the resistances of the testing circuit or the imperfections at the interface between the whisker and electrolyte. Besides, Prof. Huang also conducted growth observations and stress measurements of individual Li whiskers by utilizing in situ AFM-ETEM technique.[102] The Li growth can be divided into three stages, spheroid Li nucleation, Li growth in length, and Li collapse (**Figure 6**a–d). During this process, they discovered that the growth stress of Li whisker could reach up to 130 MPa under an applied voltage. The researchers also performed experiments involving the compression of a single lithium whisker (Figure 6e). In this process, an AFM tip was used to push the compressed whisker upward until an inclined shear band formed, indicating the occurrence of plastic yielding. The collapse of the lithium whisker was triggered by further compression.[102]

Furthermore, Prof. Sheldon and his co-workers conducted precise in situ measurement to detect the stress evolution in the Li deposition process.[103] By collecting data from films of varying thickness, they were able to differentiate between Li plating-induced stress and SEI films. The measurements conducted under different testing conditions showed that the stress was initially induced by the multiphase SEI forming on the surface of anodes (**Figure 7**a–d).[103] Additionally, they presented an analytical model that demonstrated how the stress on the surface layer significantly affected morphology evolution (Figure 7e,f). Overall, the results of this study indicated significant stress within the SEI films.

3. Stress Relief Strategy in Metal Anodes

Stress relief strategy has been put forward to solve the metal dendrite problem, which arises at the surface of electrode during

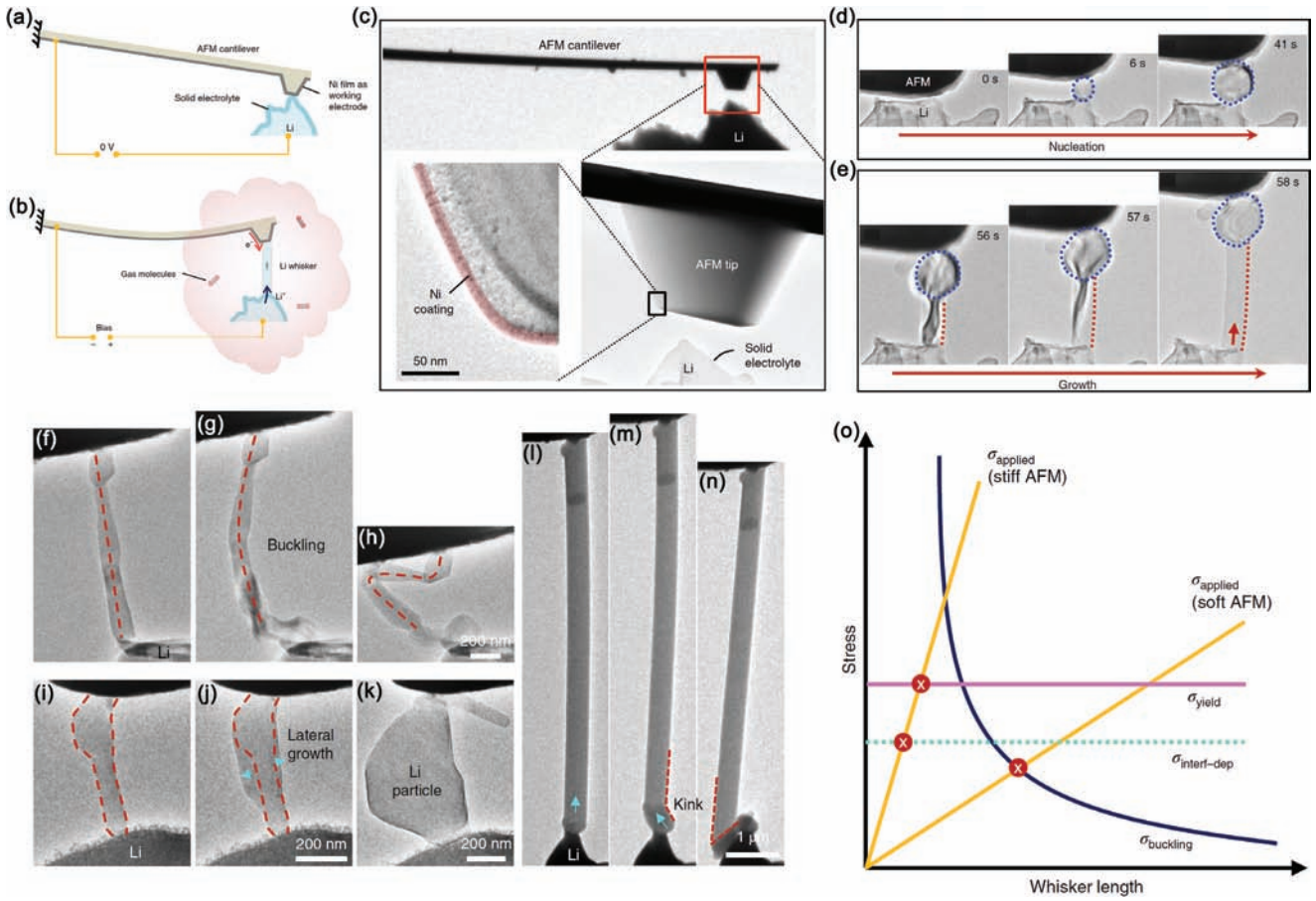

Figure 5. a) Schematic of the experimental set-up for Li deposition in AFM. b) Schematic of Li whisker growth under the AFM cantilever. c) TEM images, showing the in situ solid cell in the ETEM. d) Sequential TEM snapshots of Li particle nucleation. e) Whisker growth process. f–h) Sequential TEM snapshots, showing buckling of a Li whisker. i–k) Sequential TEM snapshots showing cessation of axial growth of the Li whisker. l–n) Sequential TEM snapshots showing kinking of the whisker. o) Critical stress versus whisker length curves for mechanical yielding (pink), buckling (blue), kinking or the stopping of axial growth (cyan). Reproduced with permission.[101] Copyright 2019, Nature Publishing Group.

metal deposition with the continuous stress accumulation. By releasing the stress induced by plating during the metal deposition process, it is possible to eliminate the formation of metal dendrites and obtain homogeneous metal deposition.

3.1. Soft Substrate Strategy

Recently, to study the effect of plating-induced stress on Li growth morphology, Prof. Jiang and his co-workers first designed experiments to plate lithium on soft Cu-polydimethylsiloxane (Cu-PDMS) substrate and directly observed the stress generation phenomenon (**Figure 8**a–f). Then, they fabricated a soft 3D host and applied for lithium anodes, achieving high CE and superior cyclic stability. The rate of dendrite growth is determined by the expression of $v = D_{Li}V_{Li}\sigma/RTr$ (v: growth rate of dendrite, D_{Li}: diffusion coefficient of Li^+, V_{Li}: molar volume of Li, σ: compressive stress, and r: dendrite radius) (Figure 8g–j), which is largely influenced by the diffusion of Li ions. When paired with a $LiFePO_4$ cathode, the full cell demonstrated exceptional cyclic performance, achieving high CE more than 99.5% (Figure 8k–m). This research highlights the importance of controlling plating-induced stress for Li dendrite suppression and improving battery performance.[84] Moreover, Prof. Luo and his co-workers raised a stress adaptable interface by utilizing the superelasticity of PDMS substrate for Li metal anode.[104] In the repeated plating-stripping processes, the substantial stress produced at the interface between the metal anode and solid electrolyte could be effectively alleviated by the strain of soft PDMS substrate. (**Figure 9**a,b). Therefore, compact interface between Li and solid electrolyte as well as an ultralong cycle life up to 5000 cycles can be obtained (Figure 9c–h). This study provides a feasible route for stabilizing the interface between lithium anode and solid electrolyte in the repeated charge–discharge processes, paving an alternative for dendrite-free anode used in all-solid state batteries.[104]

Besides, in order to attain Li storage that is highly reversible, Prof. Huang and his co-workers utilized a current collector made up of silver (Ag) nanowires coated melamine sponge (MS@AgNWs).[105] The current collector, which included lithophilic nanoseeds, and a stress-releasing soft substrate, was able to promote uniform Li deposition (**Figure 10**a–g). The resulting MS@AgNWs-Li anode demonstrated high CE of 99.1% more than 300th cycle and low voltage polarization of 10 mV. The

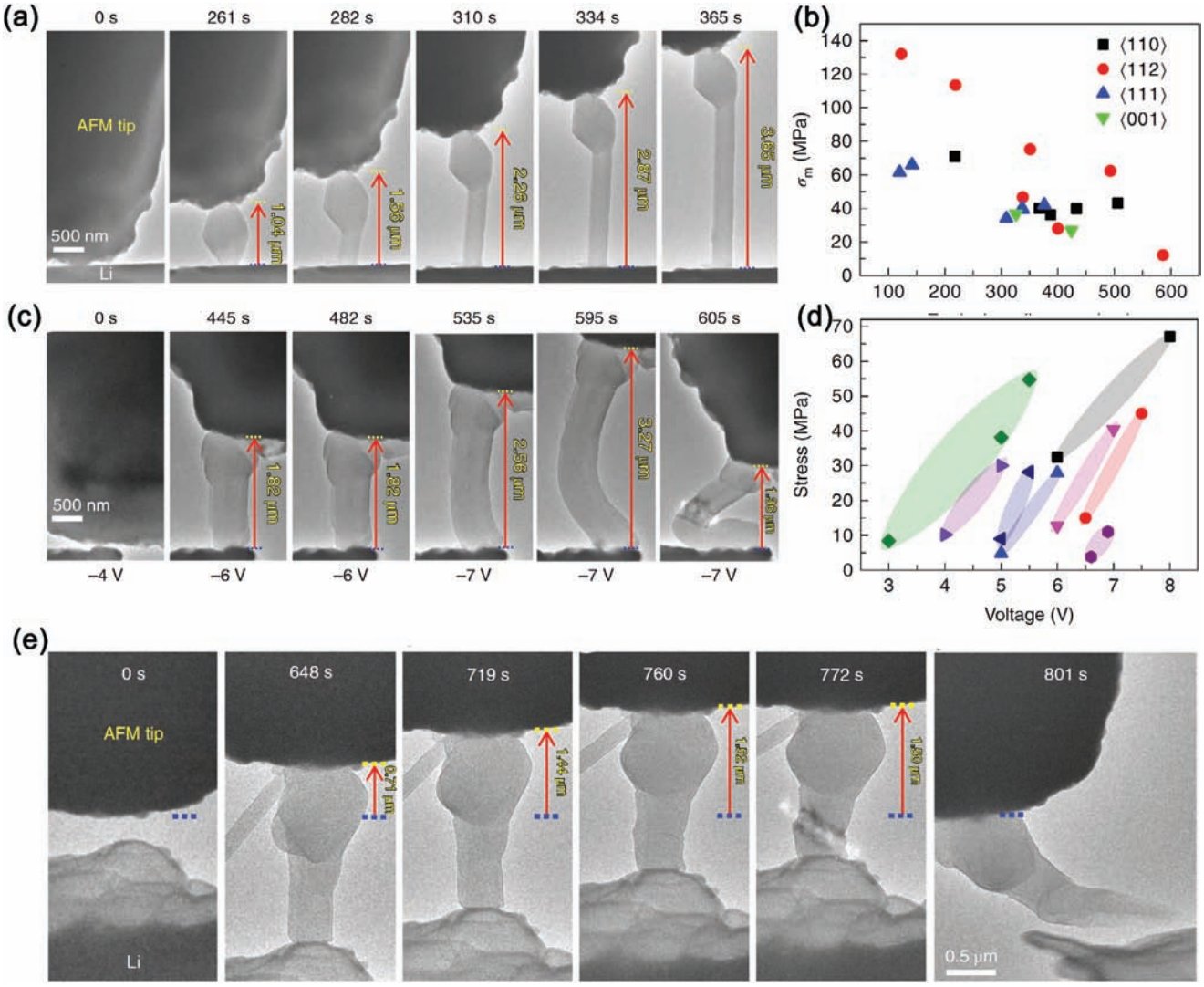

Figure 6. In situ AFM–ETEM imaging of Li whisker growth and concurrent measurement of the maximum stress in Li whiskers under applied voltages. a) A Li ball with size of 568 nm nucleated underneath the AFM tip without CNT (261 s) and then necked down to form a whisker (282 s, 310 s, 365 s). b) Plot of the maximum stress σ_m versus equivalent diameter for Li whiskers with different growth directions. c) TEM images of a whisker grown at an applied potential of −6 V (445 s), ceasing a prolonged growth time (482 s). d) Critical compressive stress (when the growth of a Li whisker stops) versus applied voltage for eight Li whiskers tested. e) In situ compression testing of as-grown Li whiskers. Reproduced with permission.[102] Copyright 2020, Nature Publishing Group.

anode also exhibited good cycle properties as well as excellent rate performance (Figure 10h,i). They proposed that the large scale production of this Li-based composite anode could be readily accomplished, creating opportunities for the development of flexible, practical lithium metal-based batteries.

Stress relief mechanism can not only function in metallic Li anode but also availably solve the Zn dendrite problems in aqueous Zn-ion batteries. Recently, Prof. Gu and Prof. Yang put forward a Zn-enriched liquid metal anode by a facile metal molten method. [85] When used as Zn anode, Zn-enriched liquid metal could availably release the huge stress during constant Zn plating processes (**Figure 11**a–c). In addition, the presence of a deformable liquid metal can significantly reduce the nucleation energy barrier of Zn to 0 V. Therefore, stress relief functional Zn anode exhibited a good electrochemical performance such as long cycle life upto 1200 h and excellent rate properties (Figure 11d–i), highly promoting the fast development of aqueous Zn ion batteries.[85] They systematically revealed the Zn nucleation and growth mechanism during the repeated stress generation and relief processes. In the Zn plating process, two types of metallic Zn deposition behaviors occurred simultaneously, namely, the uniform Zn plating ($v_{\text{uniform plating}}$) and Zn dendrite ($v_{\text{dendrite}}$) generation. To obtain a dendrite-free Zn plating anode, the formation rate of uniform Zn plating should be faster than that of dendrite generation ($v_{\text{uniform plating}} > v_{\text{dendrite}}$).[85] In the Zn-enriched liquid metal anode, the plating induced stress can be entirely released by the surface wrinkling, which makes it close to zero stress. This indicates that the formation rate of uniform Zn plating is much faster than that of Zn dendrite generation.[85]

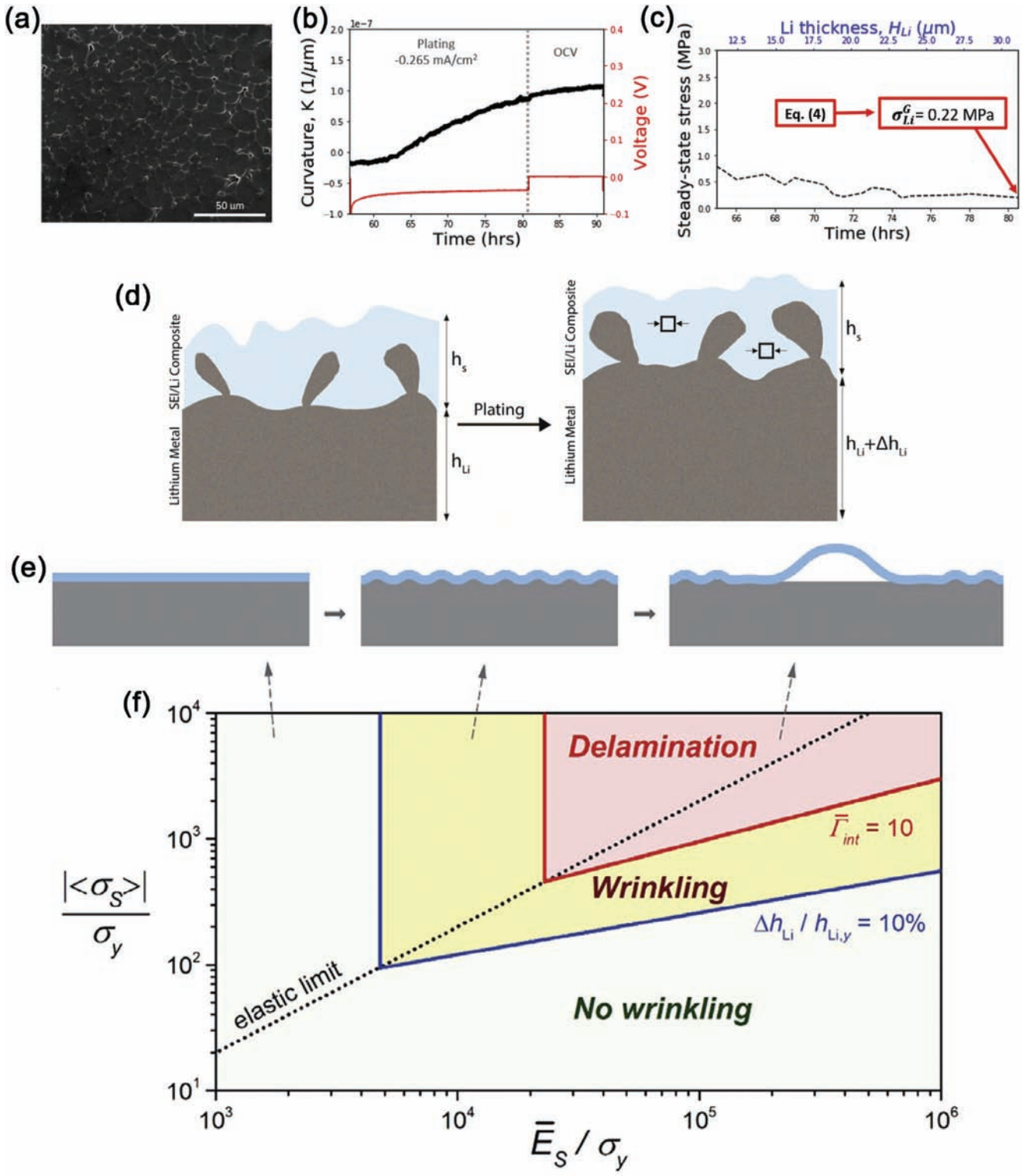

Figure 7. a) SEM image of Li film created via electrochemical deposition. Before cycling, ≈31 µm of Li was plated onto the Au current collector. b) Curvature versus time curves during initial Li film deposition. c) Steady-state stress during the latter part of the plating step in (b). d) Schematic of SEI on Li during plating. e) Schematics of SEI states on Li metal. f) SEI failure map based on analytical models of wrinkling and delamination. Reproduced with permission.[103] Copyright 2019, Elsevier Ltd.

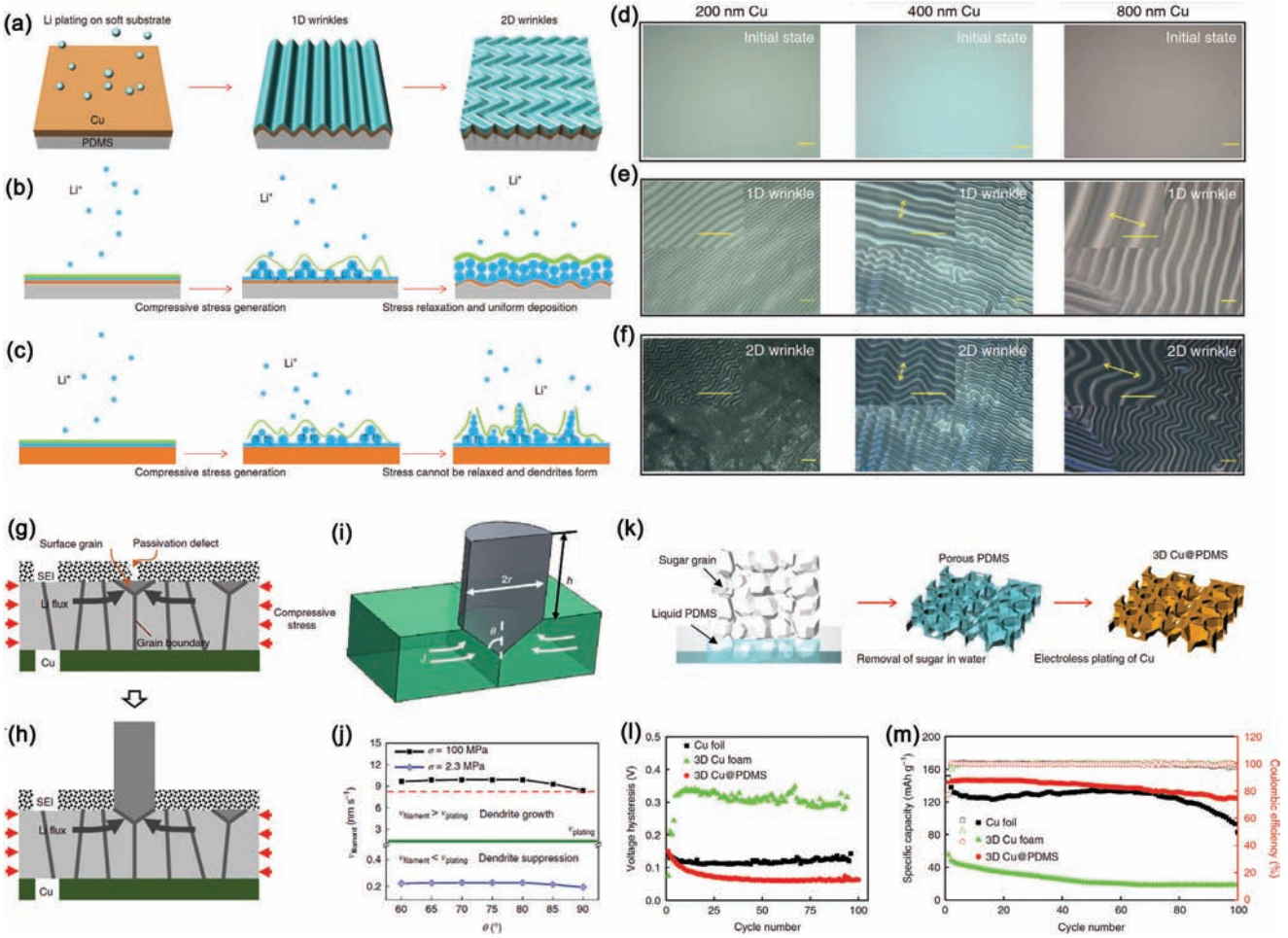

Figure 8. Cu film wrinkling during Li plating and dendrite mitigation by using soft substrate. a) Schematic of thin Cu film wrinkles on PDMS substrate, showing the compressive stress generated during Li plating. b) Schematic of Li electroplating process, during which compressive stress is initially generated, and then be released by soft substrate, and finally mitigates Li dendrite growth. c) Schematic of Li electroplating process, where the Li-plating-induced compressive stress cannot be relaxed on hard Cu foil. d) The initial flat states of the 200, 400, and 800 nm thick Cu thin-film current collectors. e) The formation of 1D wrinkles after a short period of Li plating on 200, 400, and 800 nm thick Cu current collectors. f) 2D wrinkles with approximately the same wavelength as 1D wrinkles after 1 h Li plating for all three Cu current collectors. g–h) Schematic of the stress-driven Li dendrite growth mechanism. i) Sectional image of a Li filament grown from a surface grain in a calculated filament growth rate. j) Plots of predicted Li filament growth rate $v_{filament}$ as a function of grain opening angle θ for compressive residual stress $\sigma = 100$ MPa (black squares) and 2.3 Mpa (blue diamonds). k) Fabrication procedures for 3D Cu/PDMS substrate. l) Comparison of the hysteresis of Li plating-stripping for Cu foil, 3D Cu foam and 3D Cu@PDMS substrate under a current density of 1 mA cm^{-2}. m) Cycling performance of a full cell with Cu foil, 3D Cu foam and 3D Cu@PDMS substrate under a current density of 1 mA cm^{-2} using $LiFePO_4$ as the cathode. Reproduced with permission.[84] Copyright 2018, Nature Publishing Group.

In comparison to Zn foil, Zn powder anodes offer greater versatility, but their rough surface increases the risk of corrosion and dendrite growth. Based on this, Prof. Zhang have developed a semi-liquid Zn anode (SLA) using a thickening agent (**Figure 12**a).[106] The rheological properties of the SLA effectively relieve stress induced by Zn plating, while the dual-conductive medium allows for uniform ion flux and plating/stripping throughout the anode. This SLA anode demonstrates good electrochemical behaviors and a long lifespan in a symmetric cell under high current densities and capacities (Figure 12b–h). In this study, a novel method utilizing electrode rheology is proposed to improve the stability of powder anodes, which can be applied to large-scale manufacturing processes.

3.2. Stress Relief Functioned 3D Host Strategy

Based on the above dendrite mitigation mechanism under huge stress, stress relief strategy can also be applied with other strategy such as 3D host, obtaining higher CE and better capacity retention than those of traditional strategies. Prof. Li and his co-workers proposed a strategy by combining stress relief with 3D host to horizontally release the stress generated in Li deposition processes, obtaining flat and dendrite-free Li morphology (**Figure 13**a–d).[107] A high CE more than 96% had been delivered after being cycled for 490 times as well as a nearly 100% capacity retention for full cells (Figure 13e–j). This research indicates a deep understanding of stress relief strategy, which can pave the

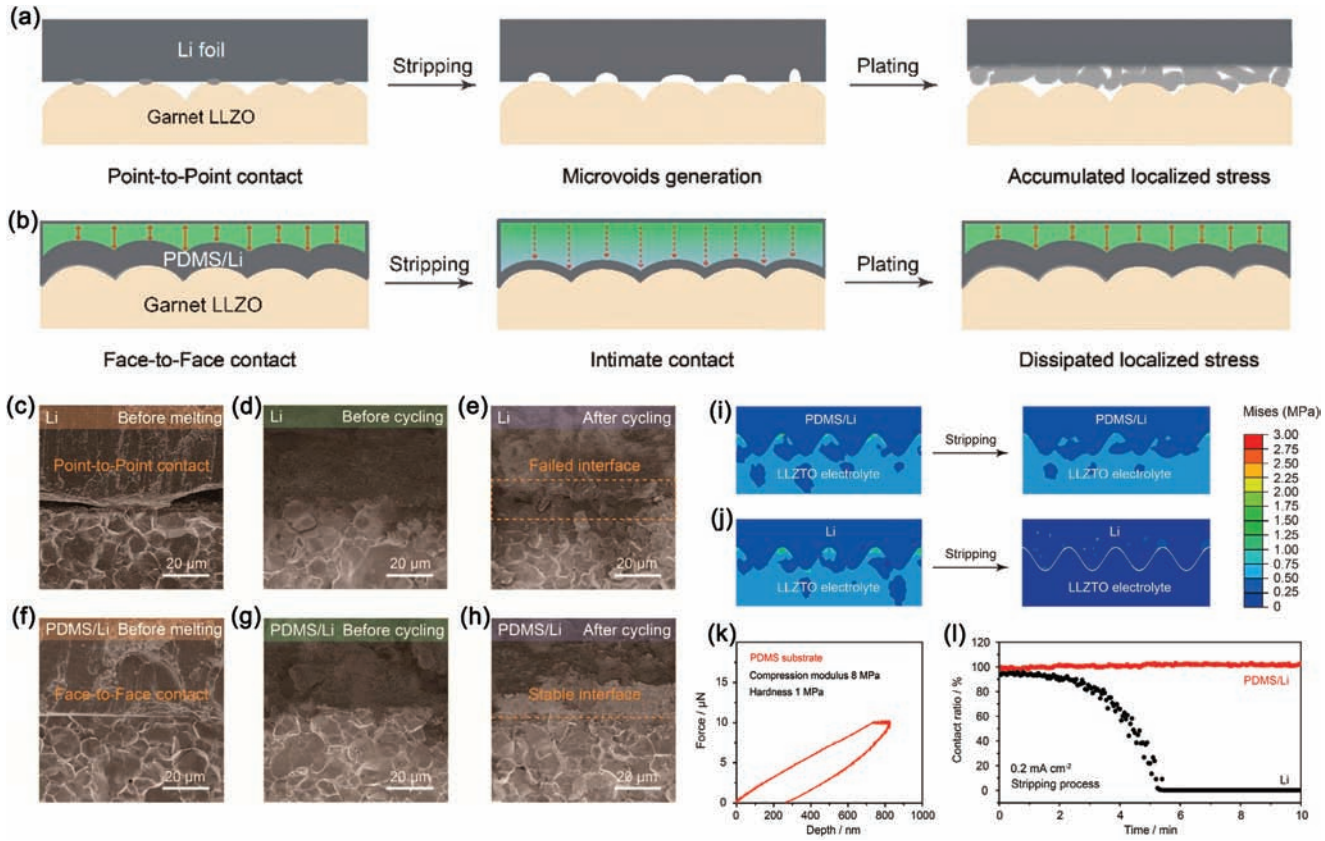

Figure 9. Schematic illustration of the stress self-adapted interface by using compressible PDMS/Li metal anode. a) Point-to-point contact between Li metal electrode and rigid Garnet electrolyte. b) Face-to-face contact between PDMS/Li metal anode and Garnet electrolyte. Comparison of the interface between c) Li and f) PDMS/Li anodes with the bare Garnet electrolytes. d,e) Li|Garnet interface and g,h) stress self-adapted PDMS/Li|Garnet interface before and after cycling. Interface variation between i) PDMS/Li and j) Li anodes and LLZTO Garnet electrolytes after Li stripping. k) Nanoindentation measurement of the hyperplastic PDMS substrate with the compression modulus of 8 MPa. l) Quantitative mathematic analysis of the contact ratio between the anodes and LLZTO Garnet electrolyte when stripping at the current density of 0.2 mA cm^{-2}. Reproduced with permission.[104] Copyright 2020, American Chemical Society.

way for the combination of stress relief strategy with 3D host. Subsequently, Prof. Liu and his team utilized a network of carbon nanotubes (CNTs) that was integrated with a soft functional polymer and PVDF, to create a coating layer on a Cu foil. This layer effectively shielded the contact between the 3D CNT framework and the electrolyte, while also releasing any internal stress accumulation in the horizontal direction (**Figure 14**a–h).[108] As a result, the Li anode-free electrode exhibited whisker-free Li deposition and improved cycling performance. The uniform current distribution induced by the CNTs and the stress mitigation caused by the soft substrate, along with a favorable SEI, contributed to a stable cycle life of the Li anode-free electrode (Figure 14i–j).

Furthermore, Prof. Zhao and his co-workers developed a patterned micro-groove structure on zinc metal anodes that effectively released plating-induced stress and inhibited Zn dendrite formation (**Figure 15**a–f).[109] The as-resulted Zn anodes, coupled with Nafion films, exhibited excellent electrochemical stability with over 1200 h of stable cycling at 10 mA cm^{-2} (Figure 15g–h). The stress relief strategy effectively inhibits Zn dendrite growth, providing valuable insights into the development of high performance aqueous Zn-ion batteries. Prof. Zhang also proposed a 3D flexible Zn anode using Zn powders via a direct 3D printing approach.[110] The resulting Zn anode showed good inherent mechanical flexibility and structural stability because of the interaction of various components, resulting in a durable and intertwined 3D structure (**Figure 16**a). Additionally, the 3D-printed customized macro holes provided adequate buffer space for stress relief to accommodate volume changes and maintain structural integrity during plating-stripping process (Figure 16b–i). The composite Zn anode obtained from this approach demonstrated exceptional long-term stability, with a lifespan of exceeding 330 h.[110] This study illustrates that 3D printing can be used to create advanced 3D host anode with stress relief functionalities for high-efficiency flexible Zn batteries, making them suitable for various flexible energy storage applications.

As a result, the soft substrate strategy and the stress relief functioned 3D host strategy are systematically discussed above. These strategies offer potential solutions to mitigate metal dendrite-related challenges. Among them, the soft substrate strategy, which involves utilizing flexible and compliant substrates, presents a more efficient approach for eliminating metal dendrites. Soft substrates, due to their pliability, can accommodate the stress generated during metal deposition, effectively

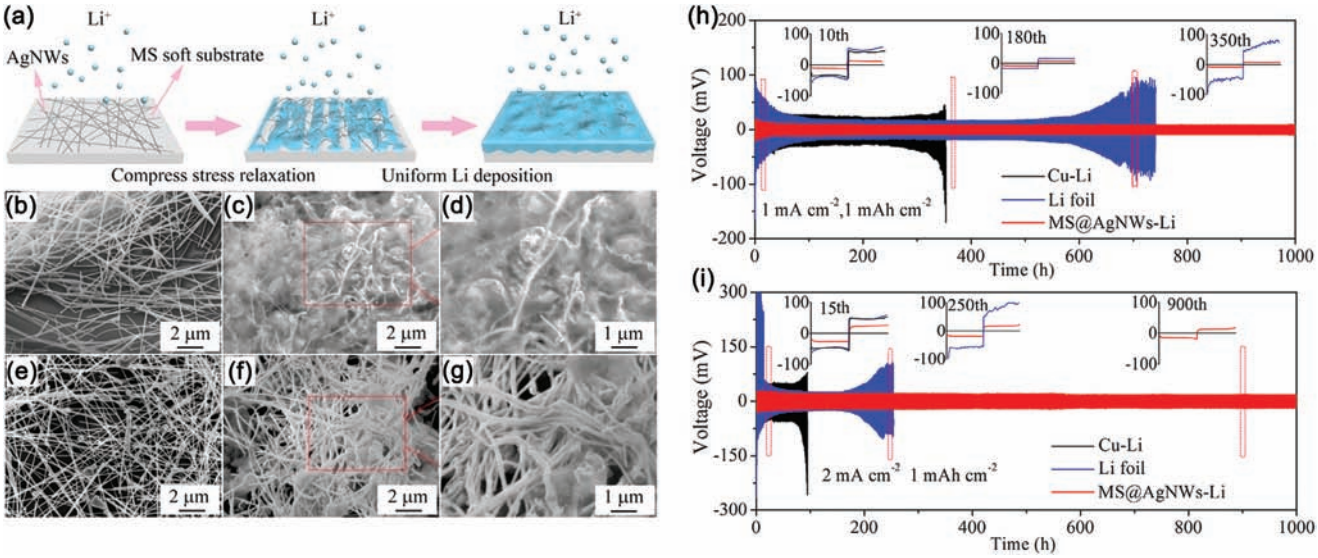

Figure 10. a) Schematic illustration of compressive stress released upon MS@AgNWs soft substrate during the Li-plating process. b) Surface SEM image of MS@AgNWs before Li deposition, and c,d) after depositing 1 mAh cm^{-2} of Li at 0.5 mA cm^{-2}. e) Surface SEM image of Cu@AgNWs before, and f,g) after depositing 1 mAh cm^{-2} of Li at 0.5 mA cm^{-2}. Galvanostatic cycling performance of MS@AgNWs-Li, Li foil and Cu–Li anodes in symmetric cells at h) 1 mA cm^{-2} and i) 2 mA cm^{-2} for 1 mAh cm^{-2}. Insets in (h) and (i) are the corresponding magnified charge–discharge voltage profiles under different cycles. Reproduced with permission.[105] Copyright 2020, American Chemical Society.

reducing the mechanical strain on the electrode surface. This stress relief minimizes the likelihood of dendrite formation and growth, promoting uniform metal deposition. Additionally, the ability of soft substrate of conforming to the evolving shape of the metal anode further hinders dendrite growth.

On the other hand, the stress relief functioned 3D host strategy, involving the integration of 3D structures into the anode, offers advantages like improved ion and electron transport. However, it might not inherently tackle the mechanical stress contributing to dendrite formation, but rather limit stress and dendrite growth. Metal dendrites can still generate within the 3D structure due to the stress accumulation during the plating process. In comparison, the soft substrate strategy has a more direct and efficient impact on dendrite elimination by addressing the stress issue at its source. It not only supports uniform metal deposition but also enhances the overall stability and safety of the anode. Therefore, considering the cruciality of mechanical aspect to dendrite formation, the soft substrate strategy emerges as a more potent solution in efficiently mitigating metal dendrite related challenges.

4. Stress Utilization in Metal Anodes

We previously discussed the negative impact of stress on metal anodes. However, it is worth noting that stress can also have a positive effect on certain physical or electrochemical properties of thin layers and nanostructures. Recently, Prof. Du and Prof. Yang utilized the property of stress in high-entropy MXene (HE-MXene) to induce uniform Li nucleation, effectively reducing the Li nucleation barrier (**Figure 17**a–e).[111] In this study, high-entropy MXene was first synthesized by the strategy of etching high-entropy MAX (Figure 17a), a groundbreaking method for preparing both high-entropy MAX and MXene materials. The high-entropy effect leads to huge lattice distortions in the structure of MXene layers, generating high stress on the surface of MXenes. This unique stress can guide homogeneous Li nucleation, significantly reducing the Li nucleation overpotential and achieving uniform Li deposition. When utilized as Li metal anodes, the high-entropy MXene exhibits ultralong cyclic performance of up to 1200 h (Figure 17i) and good deep plating-stripping properties (Figure 17j). Besides, the utilization of high-entropy MXene with significant mechanical strains can also enhance the catalytic activity and conversion efficiency of polysulfides. When applied in lithium-sulfur batteries, it has demonstrated a remarkable high-rate capability (702 mAh g^{-1} at 4C) and excellent cycle stability (360 cycles).[112] These works pave the way for fabricating more high-entropy MXenes with various components, opening up new possibilities for the utilization of stress in the energy storage applications.

5. Stress Detection Methods

For more than a century, scientists have been concerning about the impact of stress on materials. This can be traced back to Gore's discovery that electrodeposition caused the bending of plates due to differing cohesive tensions on their inner and outer surfaces. Stoney subsequently established a correlation between film stress and substrate bending, which could be determined by measuring substrate curvature or deflection.[113] Subsequent to that period, significant advancements have been made, with notable progress occurring after the 1960s when physical vapor deposition processes were conducted under high vacuum conditions. As a result, various stress detection methods have been devised, including wafer curvature, X-ray diffraction, and FIB-based techniques (Figure 3).

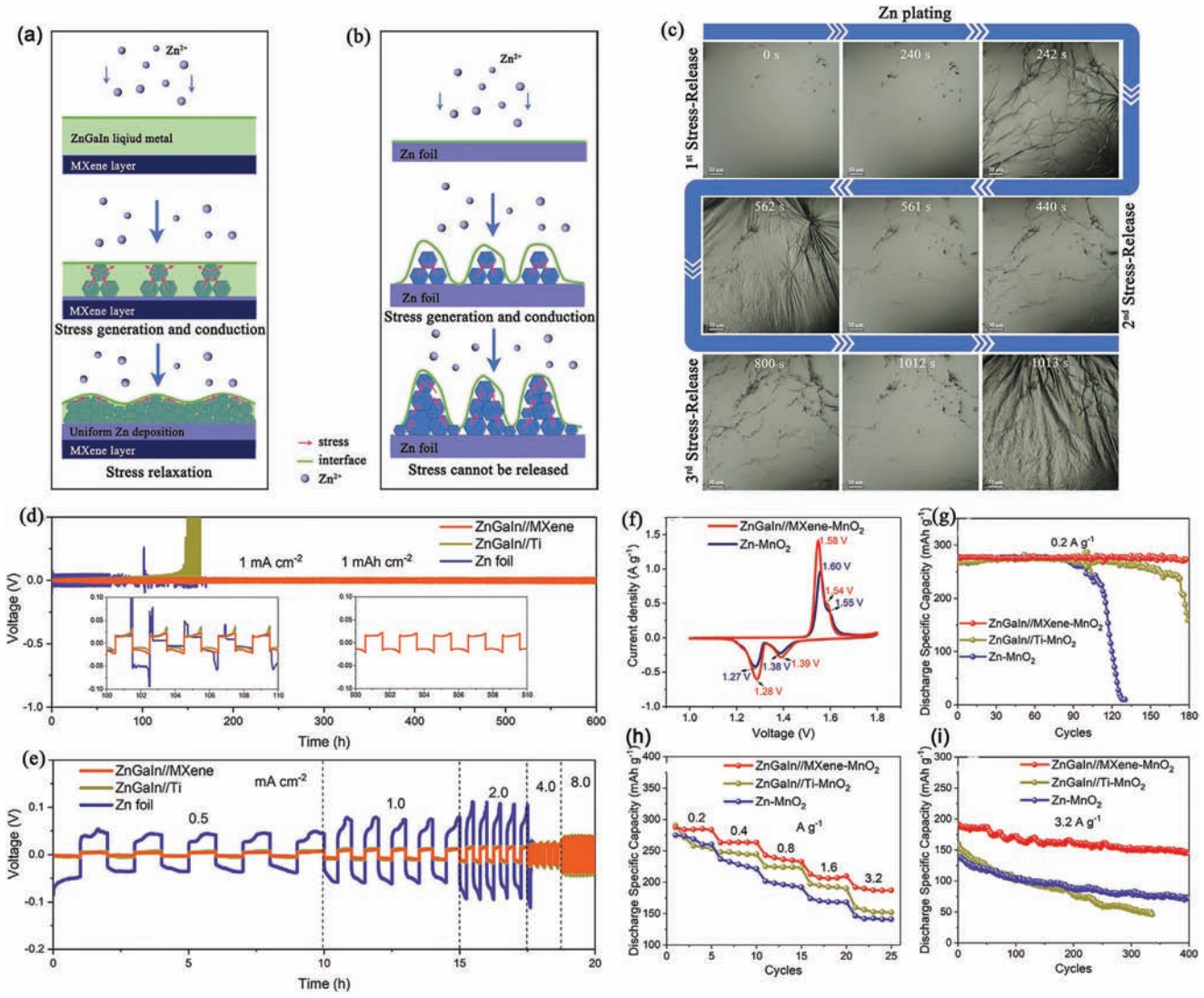

Figure 11. Schematic illustration of Zn plating mechanism on a) soft ZnGaIn//MXene metal and b) pure Zn foil. c) In situ optical microscopy visualization of Zn plating on ZnGaIn//MXene anode at different plating stages. d) Cyclic properties and e) rate performance for symmetric cells with ZnGaIn//MXene, ZnGaIn//Ti, and Zn foil anodes, respectively. Inset diagram in d) are the selected stripping–plating curves from 100 to 110 h and 500 to 510 h, respectively. f) CV curves of ZnGaIn//MXene-MnO_2 and Zn-MnO2 full cells, respectively. g) Cyclic performance of ZnGaIn//MXene-MnO_2, ZnGaIn//Ti-MnO_2, and Zn-MnO_2 full cells at 0.2 A g^{-1}. h) Rate capacities of ZnGaIn//MXene-MnO_2, ZnGaIn//Ti-MnO_2, and Zn-MnO_2 full cells at various current densities from 0.2 to 6.4 A g^{-1}. i) Cyclic performance of MnO_2-based full cells coupled with ZnGaIn//MXene, ZnGaIn//Ti, and Zn anodes at 3.2 A g^{-1}. Reproduced with permission.[85] Copyright 2022, Wiley-VCH.

5.1. Wafer Curvature

The wafer curvature technique plays a crucial role in measuring stress levels in thin films. This method involves measuring the curvature of the substrate, which is induced by stress in the thin film. Due to its ability to accurately quantify stress levels in thin films in real-time and without causing damage, the wafer curvature technique has become a popular choice among researchers and manufacturers.[114] By utilizing the well-established Stoney equation,[115] $\kappa = \frac{6\bar{\sigma}h_f}{M_s h_s^2}$, it is possible to derive a correlation between the measured curvature (j) and the average stress in the film (σ_r). This equation takes into account various parameters, including the thickness of the substrate (h_s), the biaxial modulus (M_s), and the stress-thickness product (h_f), which is measured in units of force per length. Therefore, various methods have been developed for measuring wafer curvature, including those that monitor the shape of cantilever via capacitance,[116] microbalance,[117] or interferometry[118] and those monitor the deflection of light beams reflected from the cantilever surface. Other methods involve monitoring the deflection of light beams reflected from the cantilever surface, such as monitoring a single reflected beam or the spacing between multiple reflected beams from the surface.[119] The use of a multiple-beam reflection method reduces susceptibility to sample vibration due to the determination of curvature through the change in spacing

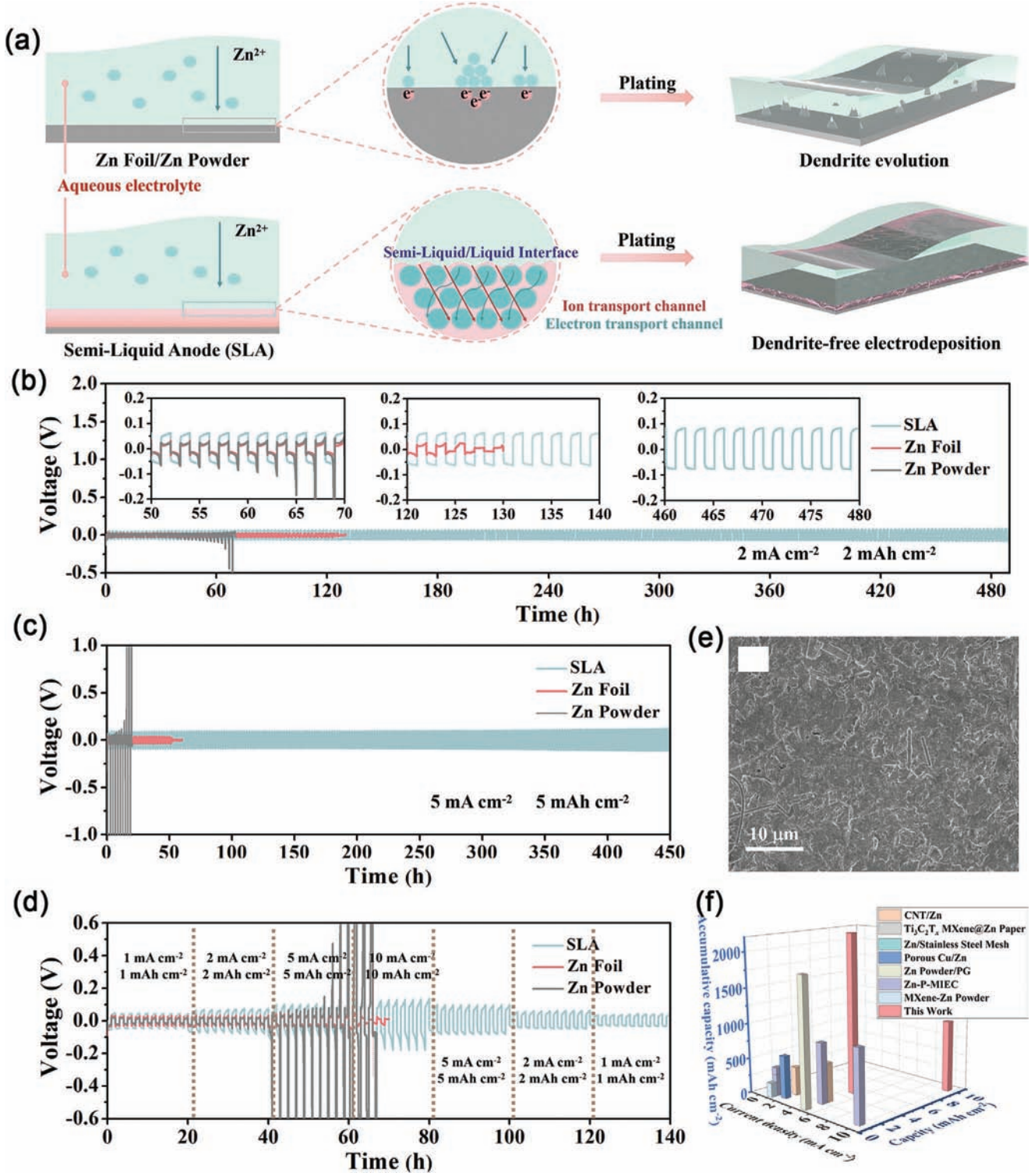

Figure 12. a) Schematic illustrations of morphology evolution of SLA and Zn foil/Zn powder anodes. Cyclic performance of SLA, Zn foil, and Zn powder, respectively, at b) 2 mA cm^{-2}, 2 mAh cm^{-2} and c) 5 mA cm^{-2}, 5 mAh cm^{-2}. d) Rate performance of SLA, Zn foil, and Zn powder, respectively. e) SEM images of SLA anode after cycling for 100 h. f) Performance comparison of SLA and other synthetic Zn anodes in terms of current densities, specific capacities, and cumulative capacities. Reproduced with permission.[106] Copyright 2023, Wiley-VCH.

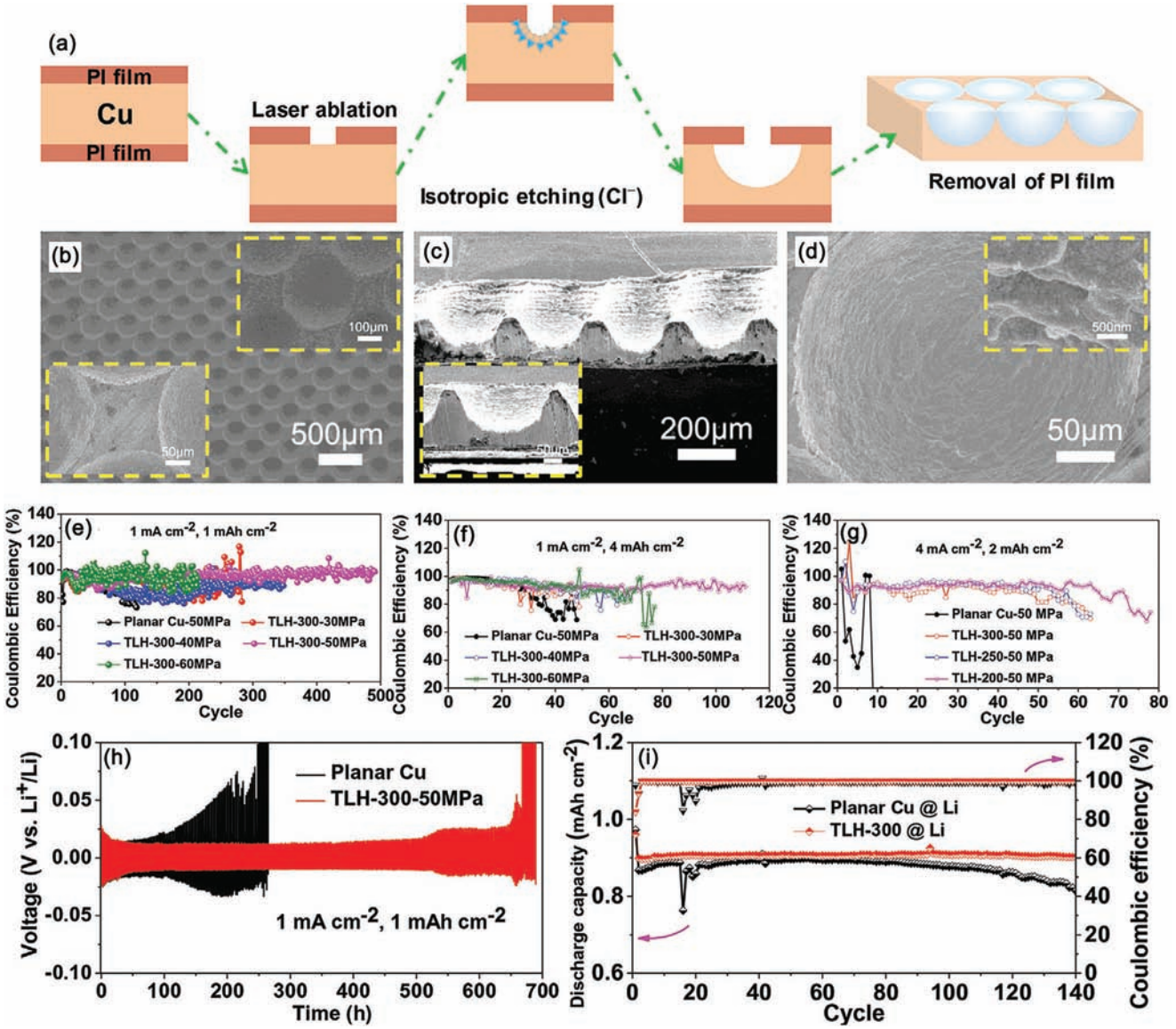

Figure 13. a) Schematic illustration of the fabrication process of TLH electrode. b) Front SEM image of the TLH-300 electrode. c) Cross-sectional SEM image of the TLH electrode. d) SEM image of the obtained lithiophilic hemisphere of TLH electrode. CE of e) and f) planar Cu electrode with packaging pressure of 50 MPa, and TLH-300 electrode with packaging pressure of 30, 40, 50, and 60 MPa. g) CE of planar Cu electrode and TLH electrodes with different diameters of the hemisphere under the same package pressure (50 MPa). h) Symmetrical cell test of planar Cu and TLH-300 electrodes at 1 mA cm^{-2} with Li capacity of 1 mAh cm^{-2}. i) Cycling performance of the Li deposited planar Cu and TLH-300 electrodes matched with LFP cathode. Reproduced with permission.[107] Copyright 2020, Wiley-VCH.

between reflected beams. In addition, a multiple-beam optical stress sensor (MOSS) is particularly useful for measurements taken within situations where there is fluid flow or convection that may affect the accuracy of measurements, such as during electrochemical deposition.[120]

5.2. FIB-Based Methods

Advancements in focused ion beam (FIB) technology, combined with scanning electron microscopy (SEM) and digital image correlation (DIC), have enabled submicron-scale measurement of residual stress in materials.[121] The FIB-DIC method involves incremental FIB milling, in situ SEM imaging, and full-field strain analysis using DIC and finite element (FE) modeling. This method has been established as the most effective for achieving submicron spatial resolutions in analyzing residual stress in thin nanostructured layers. Various milling relaxation geometries including hole drilling, ring-core, as well as slitting have been proposed. Among them, the ring-core geometry has gathered particular interest because of its high spatial resolution, and as it enables full 2D stress mapping with high precision. The appropriate selection of a milling geometry is crucial for obtaining a precise and detailed analysis of residual stress profile with submicron

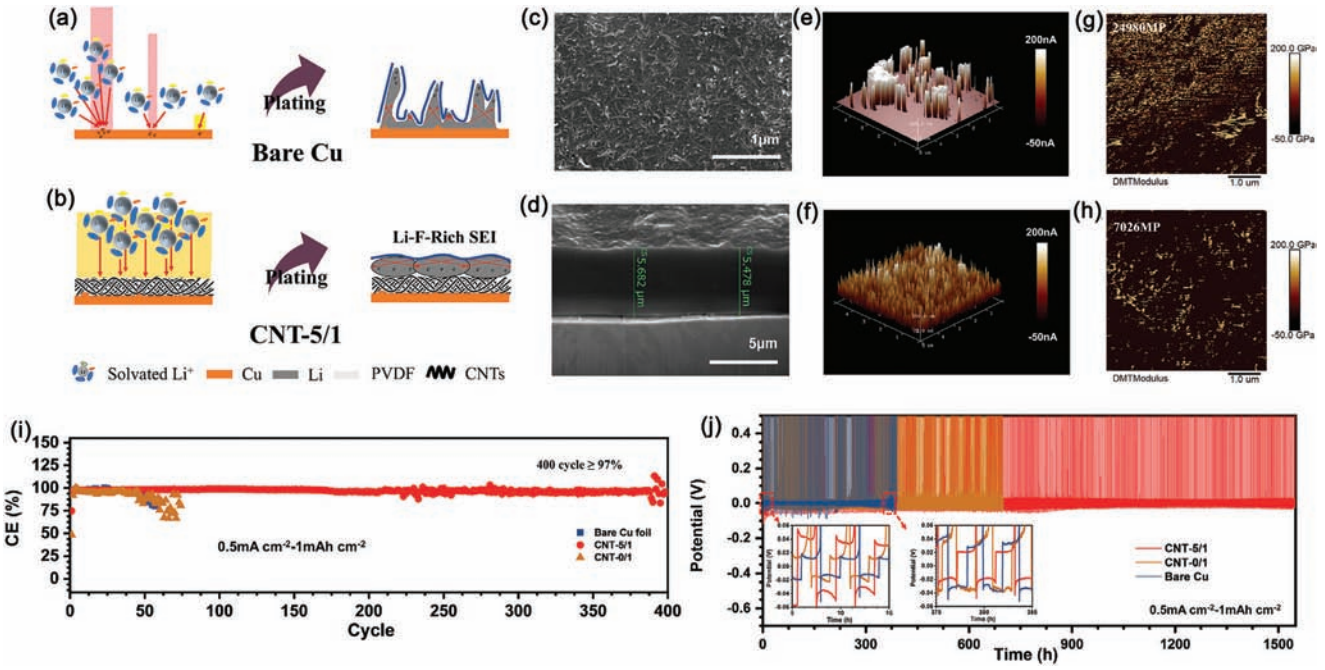

Figure 14. Schematic diagrams showing the morphology of electrodeposited Li on bare a) Cu foil and b) CNT-5/1. c) Top view and d) cross-section view SEM images of CNT-5/1. Surface current distribution and DMT modulus over e–g) Cu and f–h) CNT-5/1 by AFM characterization. i) Comparison of CE of Li plating/stripping with capacity of 1 mAh cm^{-2}. j) Comparison of voltage profiles of Li plating/stripping on bare Cu, CNT-0/1, and CNT-5/1 with a capacity of 1 mAh cm^{-2} at 0.5 mA cm^{-2}. Reproduced with permission.[108] Copyright 2022, American Chemical Society.

resolution, as well as the in-plane stress tensor, stress within individual grains with varying crystal orientation, and the material's Poisson's ratio. However, it is essential to select the appropriate geometry in line with the material properties and measurement objectives. The FIB-DIC method has been validated against other standard measurement techniques, including XRD and micro-Raman methods, and has been found to provide comparable results with minor differences, which could be attributed to factors such as the elastic modulus of the film, and probing volumes of the techniques used. The FIB-DIC method has several advantages, such as providing detailed information on the distribution of residual stress both at the surface and in-depth of the sample.

5.3. X-ray Diffraction

X-ray diffraction is used to determine residual stress and gradients in films.[122] The "$sin^2\psi$ method" is a commonly used approach to calculate residual stress from X-ray elastic strains. This method employs X-ray elastic constants to determine mechanical elastic constants for isotropic materials. Lattice spacing is measured using a two-circle diffractometer, glancing angle scan, or four-circle diffractometer. However, these methods only work for thin films with a random grain orientation. If the material exhibits crystallographic texture or stress gradients, more complex analysis is required. Thus, one method utilized for analyzing the nanoscale variation of residual stress and microstructure in thin films is cross-sectional transmission electron microscopy (TEM).[123] This technique involves taking a cross-sectional sample of the thin film and analyzing it using a TEM to obtain detailed information about the microstructure and residual stress distribution at the nanoscale level. The technique enables the determination of grain orientations and their misorientations, grain sizes, and the variation of residual stress with depth.

6. Conclusion and Outlook

In conclusion, the formation of metal dendrites during repeated plating-stripping processes remains a significant challenge that hinders the practical application of metal anodes (Li/Na/Zn) in rechargeable batteries. The issues related to low Coulombic efficiency, poor cycle life, and safety concerns associated with dendrite formation can be addressed by adopting the stress relief strategies. The stress generated during metal deposition is a major contributor to dendrite formation, and stress relief strategies, such as those discussed earlier, can eliminate metal dendrites and enhance the properties and safety of metal anodes. Stress detection methods, including wafer curvature, FIB-based techniques, and X-ray diffraction, are used to measure stress levels in the process of metal deposition, and the stress behavior of films can be classified into two types based on their stress-thickness relationship.

We have explored stress generation and evolution mechanisms in metal dendrites, with a focus on metallic Sn and Li metals, and highlighted the development of various anodes, including metallic Li anodes, Zn-enriched liquid metal anodes, patterned micro-groove structure Zn anodes, semi-liquid Zn anodes, 3D-printed flexible Zn anodes, and 3D porous carbon fiber anodes. Besides, stress can also be utilized in high-entropy MXene to induce Li nucleation during Li deposition process. Overall, stress relief strategies have great potential to improve the electrochemical performance of metal anodes and create rechargeable

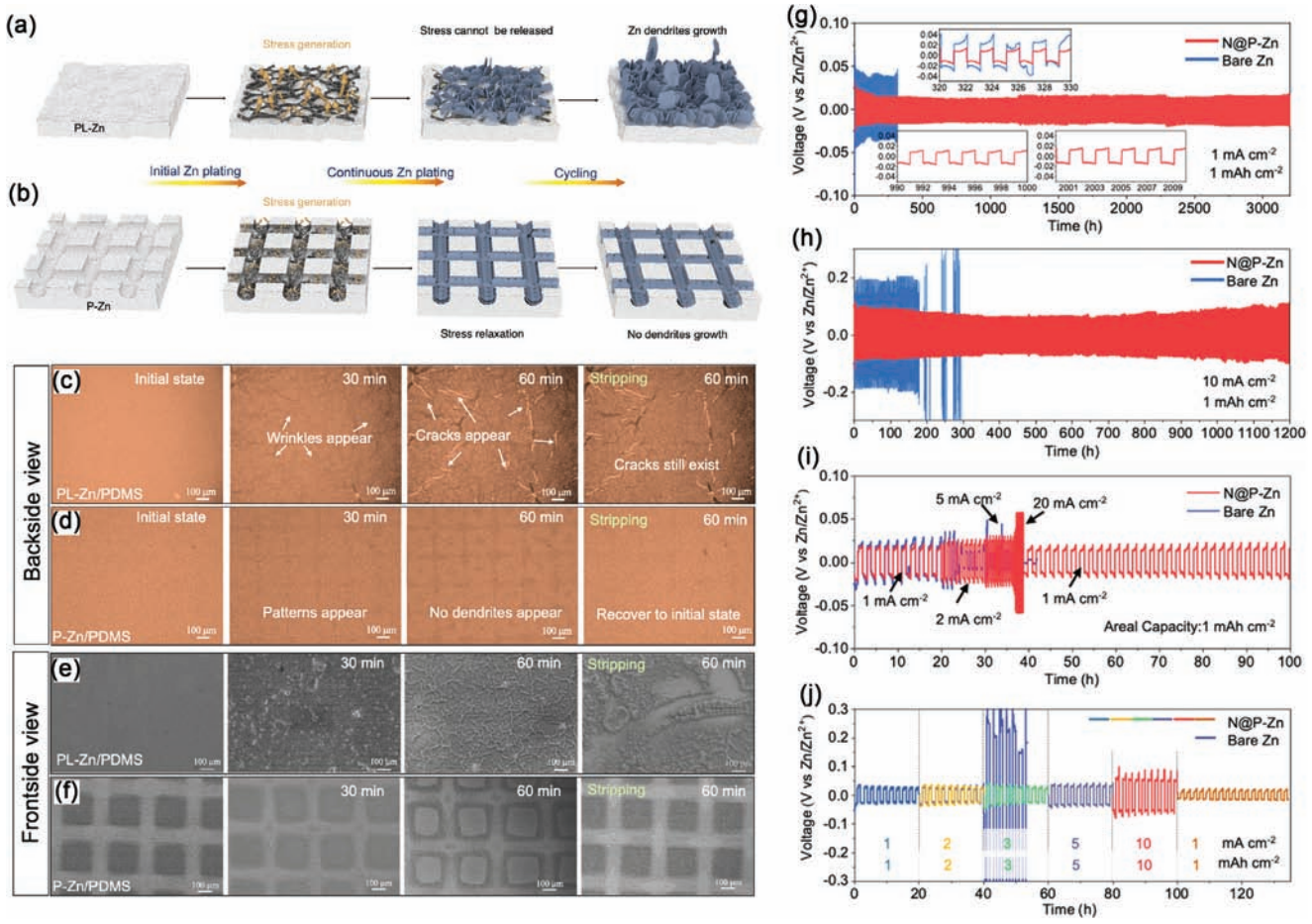

Figure 15. Schematic illustrations of Zn-plating-induced stress and its effect on Zn plating/stripping behavior on a) PL-Zn and b) P-Zn. In situ optical microscope observations of the backsides for c) PL-Zn/PDMS and d) P-Zn/PDMS. Ex situ SEM images of frontside for e) PL-Zn/PDMS and f) P-Zn/PDMS. (g,h) Voltage profiles of N@PZn and bare Zn-based symmetric cells. i,j) Rate performances of N@PZn and bare Zn-based symmetric cells. Reproduced with permission.[109] Copyright 2022, Elsevier Ltd.

batteries with improved properties and longer cycle life for practical applications. While stress relief strategies have shown great promise in mitigating metal dendrite formation and improving the properties of rechargeable batteries with metal anodes, there are still several challenges that need to be addressed:

1) One of the main challenges is developing stress relief strategies that are effective over the entire range of operating conditions of the batteries, including high current densities, high charging rates, and different temperatures. Additionally, while stress relief strategies have been effective in laboratory-scale experiments, their implementation in large-scale manufacturing processes and practical battery systems remains a challenge, particularly concerning aspects like compatibility with existing battery technologies, scalability, and cost considerations. As for the compatibility with existing battery technologies, integrating stress relief techniques into practical battery systems requires compatibility with existing battery designs, manufacturing processes, and materials. It may be challenging to incorporate new stress relief strategies without significantly altering the established battery architecture. Besides, the stress relief techniques employed should also be compatible with the electrolyte used in the battery system. They should not adversely react with or degrade the electrolyte, as it plays a critical role in ion transport and overall battery performance. Besides, stress relief techniques should be scalable to meet the production demands of large-scale battery manufacturing. Ensuring that the techniques can be applied consistently and cost-effectively across high-volume production processes is essential. The implementation of stress relief techniques should be economically viable, without significantly increasing the production costs of the batteries. It is important to balance the cost-effectiveness of the techniques with their potential benefits in terms of improved performance and safety.
2) Another area for future research is improving the understanding of the mechanisms of stress generation and accumulation in metal dendrites, particularly for emerging metal anodes such as Na and potassium (K). Besides, as for different metal anodes such as Li, Na, and Zn, they have distinct properties and behavior during dendrite formation. Stress relief techniques need to be evaluated and optimized for each specific metal anode to ensure effective dendrite inhibition. This understanding of the mechanisms of stress generation and

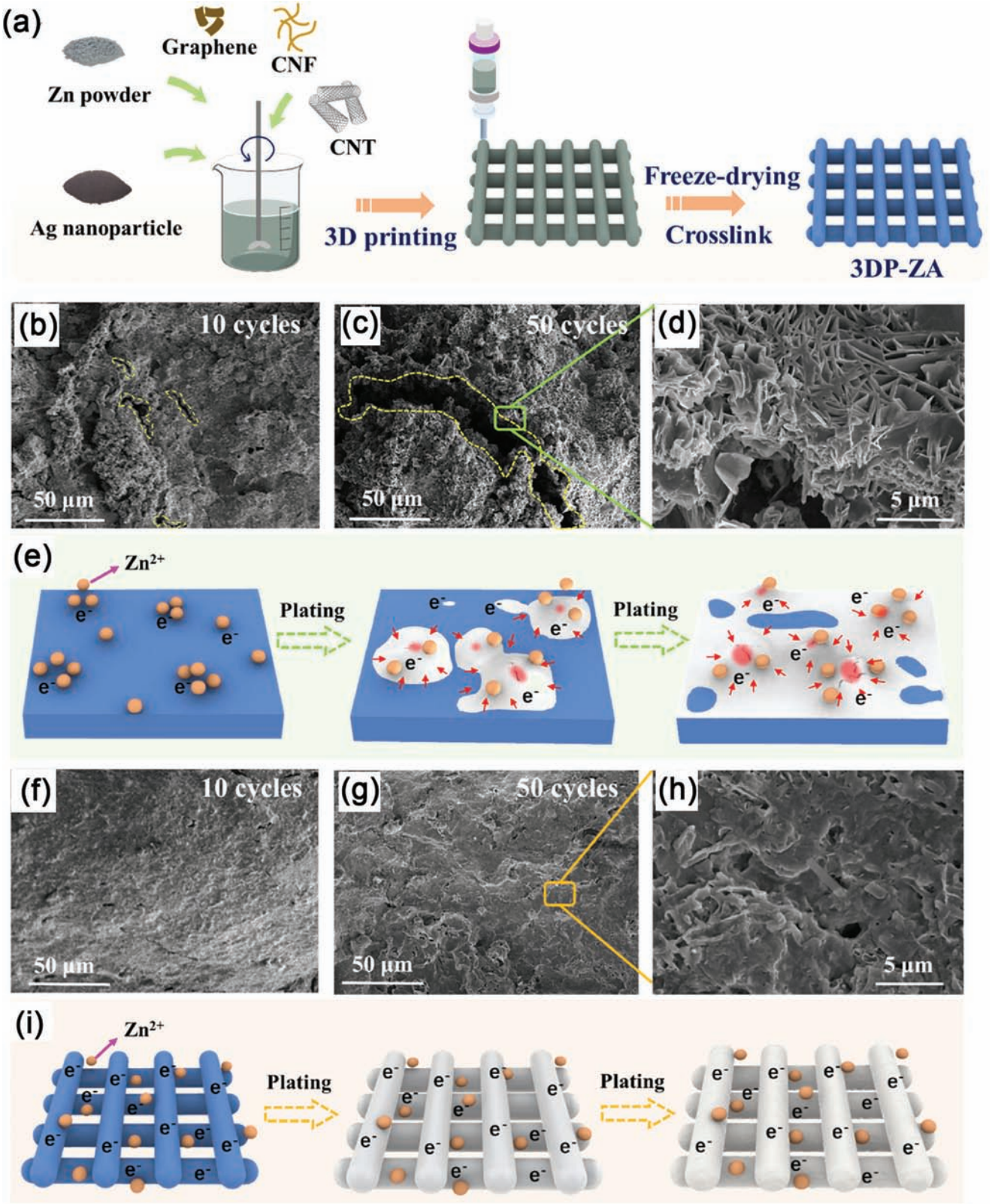

Figure 16. a) The schematic illustration of the preparation process of the 3DP-ZA anode. SEM images of Bulk-ZA anode after b) 10 cycles and c,d) 50 cycles. e) The illustration of the deposition process of Bulk-ZA anode. SEM images of 3DP-ZA anode after f) 10 cycles and f,g) 50 cycles. i) Schematic illustration of the deposition process of 3DP-ZA anode. Reproduced with permission.[110] Copyright 2022, Elsevier Ltd.

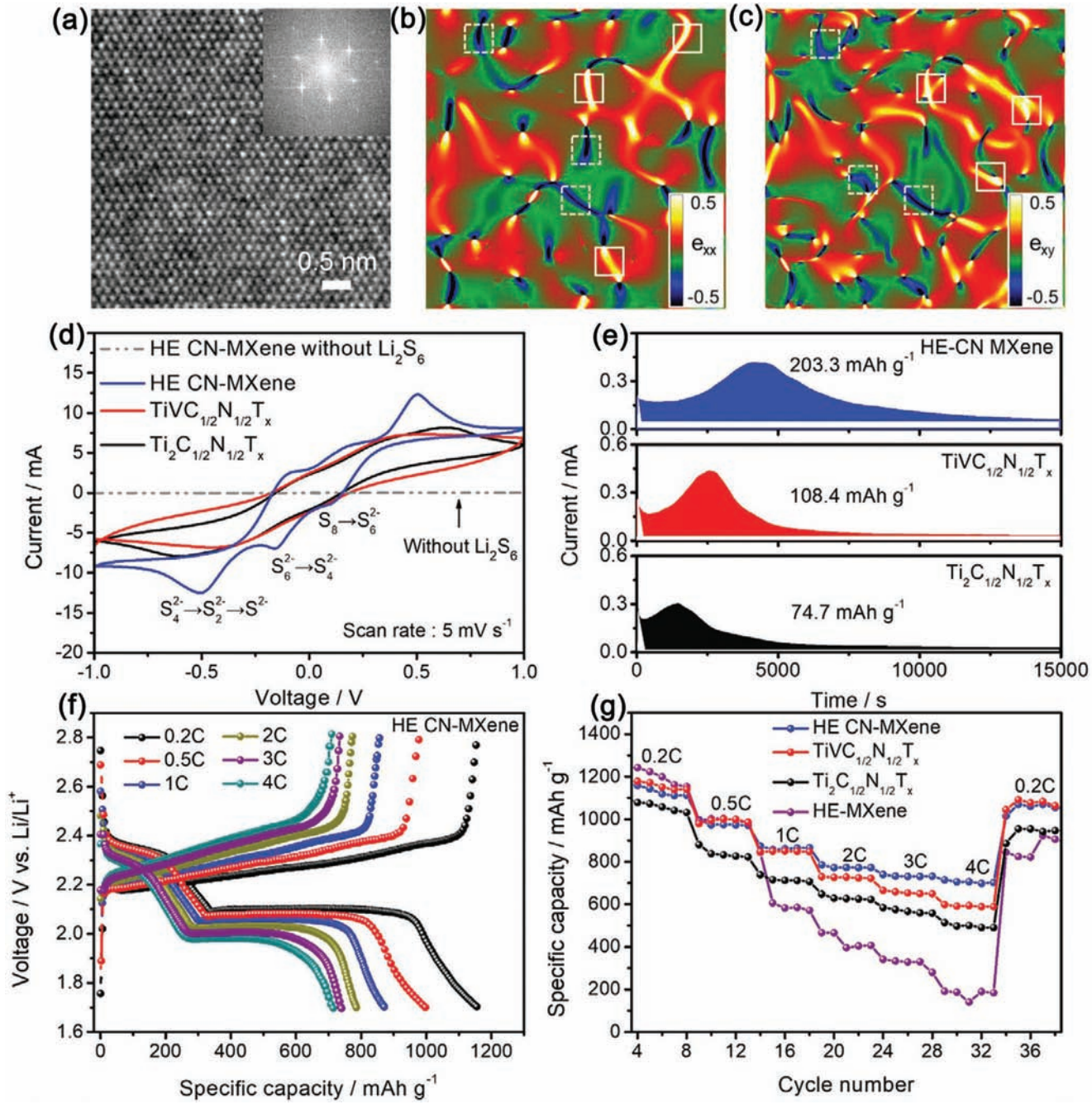

Figure 17. a) Schematic illustration of the preparation of HE-MXene from HE-MAX $(Ti_{1/5}V_{1/5}Zr_{1/5}Nb_{1/5}Ta_{1/5})_2AlC$ via the F-containing etching approach. b) XRD patterns of MXenes with Ti, V, Zr, Nb, and Ta species. c) SEM and d) HRTEM and inset in (d) the corresponding fast Fourier transform (FFT) images of HE-MXene atomic layers. The inset in (c) shows the dispersion of HE-MXene layers. e) Atomic-resolution STEM image and enlarged view of areas I and II of HE-MXene. f,g) Strain distribution of e_{xx} (f) and e_{xy} (g) for HE-MXene. h) Nucleation overpotential on the voltage profile of Li plating on HE-MXene at 0.05 mA cm^{-2}. i) Galvanostatic cycling performance of symmetric cells with HE-MXene–Li, $TiNbT_x$–Li, Ti_2CT_x-Li, and bare Li at 1.0 mA cm^{-2} and 1.0 mAh cm^{-2}. j) Galvanostatic cycling of HE-MXene-Li at different deep stripping and plating capacities for 5, 10, and 20 mAh cm^{-2} at 1.0 mA cm^{-2}. Reproduced with permission.[111] Copyright 2021, Wiley-VCH.

accumulation in metal dendrites will enable the development of more effective stress relief strategies tailored to specific metals.

3) Last, there is a need for more research into the long-term stability and safety of rechargeable batteries with metal anodes, particularly in high-stress environments. Stress relief techniques should not compromise the long-term stability and durability of the battery system. It is crucial to assess the impact of stress relief strategies on the overall performance, cycle life, and safety of the battery over extended periods of

usage. This will require the development of new methods for predicting and monitoring stress levels in batteries over their lifetime.

Addressing these limitations and challenges is crucial for successful implementation of stress relief techniques in practical battery systems and future research. However, further research is required to overcome the remaining challenges and enable the widespread implementation of stress relief techniques. Improved stress relief strategies, a better understanding of stress generation and accumulation mechanisms, long-term stability and safety studies will be essential in achieving this goal. We believe that the stress relief can be a general strategy to solve dendrite issues in metal anodes (Li/Na/K and Zn).

Acknowledgements

This work is supported partially by project of State Key Laboratory Of Alternate Electrical Power System With Renewable Energy Sources (LAPS21004 and LAPS202114), National Natural Science Foundation of China (Grant nos. 52102203, 52272200, 51972110, 52102245, 52072121 and 52202204), Huaneng Group Headquarters Science and Technology Project (HNKJ20-H88).

Conflict of Interest

The authors declare no conflict of interest.

Keywords

metal anodes, metal dendrites, nucleation and growth, stress evolution, stress relief

Received: July 1, 2023
Revised: August 24, 2023
Published online: September 15, 2023

[1] K. Yoon, S. Lee, K. Oh, K. Kang, *Adv. Mater.* **2022**, *34*, 2104666.
[2] M. Zhang, D. A. Kitchaev, Z. Lebens-Higgins, J. Vinckeviciute, M. Zuba, P. J. Reeves, C. P. Grey, M. S. Whittingham, L. F. J. Piper, A. van der Ven, Y. S. Meng, *Nat. Rev. Mater.* **2022**, *7*, 522.
[3] Y. Zhang, Z. Cao, S. Liu, Z. Du, Y. Cui, J. Gu, Y. Shi, B. Li, S. Yang, *Adv. Energy Mater.* **2022**, *12*, 2103979.
[4] J. Gu, H. Chen, Y. Shi, Z. Cao, Z. Du, B. Li, S. Yang, *Adv. Energy Mater.* **2022**, *12*, 2201181.
[5] J. Liu, M. Wu, X. Li, D. Wu, H. Wang, J. Huang, J. Ma, *Adv. Energy Mater.* **2023**, *13*, 2300084.
[6] S. Zhang, M. Ye, Y. Zhang, Y. Tang, X. Liu, C. C. Li, *Adv. Funct. Mater.* **2023**, *33*, 2208230.
[7] R. F. Ziesche, N. Kardjilov, W. Kockelmann, D. J. L. Brett, P. R. Shearing, *Joule* **2022**, *6*, 35.
[8] Q. Zhao, R. Zhou, C. Wang, J. Kang, Q. Zhang, J. Liu, Y. Jin, H. Wang, Z. Zheng, L. Guo, *Adv. Funct. Mater.* **2022**, *32*, 2112711.
[9] Q. Zhao, R. Wang, X. Hu, Y. Wang, G. Lu, Z. Yang, Q. Liu, X. Yang, F. Pan, C. Xu, *Adv. Sci.* **2022**, *9*, 2102215.
[10] V. Raj, V. Venturi, V. R. Kankanallu, B. Kuiri, V. Viswanathan, N. P. B. Aetukuri, *Nat. Mater.* **2022**, *21*, 1050.
[11] Y. Wang, J. Liang, X. Song, Z. Jin, *Energy Storage Mater.* **2023**, *54*, 732.
[12] Y. Li, Q. Zhu, M. Xu, B. Zang, Y. Wang, B. Xu, *Adv. Funct. Mater.* **2023**, *33*, 2213416.
[13] A. Wang, K. Zhang, L. Zhang, Q. Ma, S. Zhou, Q. Jiang, Z. Hu, J. Luo, *Small* **2023**, *19*, 2301166.
[14] S. Zhou, C. Fu, Z. Chang, Y. Zhang, D. Xu, Q. He, S. Chai, X. Meng, M. Feng, Y. Zhang, J. Lin, A. Pan, *Energy Storage Mater.* **2022**, *47*, 482.
[15] J. Zhang, R. He, Q. Zhuang, X. Ma, C. You, Q. Hao, L. Li, S. Cheng, L. Lei, B. Deng, X. Li, H. Lin, J. Wang, *Adv. Sci.* **2022**, *9*, 2202244.
[16] S. Qian, C. Xing, M. Zheng, Z. Su, H. Chen, Z. Wu, C. Lai, S. Zhang, *Adv. Energy Mater.* **2022**, *12*, 2103480.
[17] D. Li, C. Xie, Y. Gao, H. Hu, L. Wang, Z. Zheng, *Adv. Energy Mater.* **2022**, *12*, 2103480.
[18] J. Jiao, G. Lai, L. Zhao, J. Lu, Q. Li, X. Xu, Y. Jiang, Y.-B. He, C. Ouyang, F. Pan, H. Li, J. Zheng, *Adv. Sci.* **2022**, *9*, 2105574.
[19] C. Bao, C. Zheng, M. Wu, Y. Zhang, J. Jin, H. Chen, Z. Wen, *Adv. Energy Mater.* **2023**, *13*, 2204028.
[20] B. Li, S. Liu, Y. Geng, C. Mao, L. Dai, L. Wang, S. C. Jun, B. Lu, Z. He, J. Zhou, *Adv. Funct. Mater.* **2023**, https://doi.org/10.1002/adfm.202214033.
[21] I. Yang, J.-h. Jeong, J. Y. Seok, S. Kim, *Adv. Energy Mater.* **2023**, *13*, 2202321.
[22] L. Zhao, Z. Wu, Z. Wang, Z. Bai, W. Sun, K. Sun, *ACS Nano* **2022**, *16*, 20891.
[23] G. Lin, K. Jia, Z. Bai, C. Liu, S. Liu, Y. Huang, X. Liu, *Adv. Funct. Mater.* **2022**, *32*, 2207969.
[24] D. Han, X. Wang, Y.-N. Zhou, J. Zhang, Z. Liu, Z. Xiao, J. Zhou, Z. Wang, J. Zheng, Z. Jia, B. Tian, J. Xie, Z. Liu, W. Tang, *Adv. Energy Mater.* **2022**, *12*, 2201190.
[25] W. Bao, R. Wang, C. Qian, M. Li, K. Sun, F. Yu, H. Liu, C. Guo, J. Li, *ACS Nano* **2022**, *16*, 17454.
[26] J. Ke, Z. Wen, Y. Yang, R. Tang, Y. Tang, M. Ye, X. Liu, Y. Zhang, C. C. Li, *Adv. Funct. Mater.* **2023**, *26*, 2301129.
[27] C. Fang, B. Lu, G. Pawar, M. Zhang, D. Cheng, S. Chen, M. Ceja, J.-M. Doux, H. Musrock, M. Cai, *Nat. Energy* **2021**, *6*, 987.
[28] Z. Zhang, S. Guan, S. Liu, B. Hu, C. Xue, X. Wu, K. Wen, C.-W. Nan, L. Li, *Adv. Energy Mater.* **2022**, *12*, 2103332.
[29] Q. Pang, J. Meng, S. Gupta, X. Hong, C. Y. Kwok, J. Zhao, Y. Jin, L. Xu, O. Karahan, Z. Wang, S. Toll, L. Mai, L. F. Nazar, M. Balasubramanian, B. Narayanan, D. R. Sadoway, *Nature* **2022**, *608*, 704.
[30] S. Li, J. Huang, Y. Cui, S. Liu, Z. Chen, W. Huang, C. Li, R. Liu, R. Fu, D. Wu, *Nat. Nanotechnol.* **2022**, *17*, 613.
[31] M. J. Lee, J. Han, K. Lee, Y. J. Lee, B. G. Kim, K.-N. Jung, B. J. Kim, S. W. Lee, *Nature* **2022**, *601*, 217.
[32] J. Chen, D. Li, K. Lin, X. Ke, Y. Cheng, Z. Shi, *J. Power Sources* **2022**, *540*, 231603.
[33] Y. Lee, B. Ma, P. Bai, *Energy Environ. Sci.* **2020**, *13*, 3504.
[34] S. Li, M. Jiang, Y. Xie, H. Xu, J. Jia, J. Li, *Adv. Mater.* **2018**, *30*, 1706375.
[35] J. Yun, J. Moon, G. H. Eom, J. moon, J. H. Kim, M.-S. Park, J.-W. Lee, S. X. Dou, *Nano Energy* **2022**, *95*, 106999.
[36] X.-Y. Yue, Q.-Y. Zhou, J. Bao, C. Ma, S.-Y. Yang, X.-L. Li, D. Sun, F. Fang, X.-J. Wu, Y.-N. Zhou, *Adv. Funct. Mater.* **2021**, *31*, 2008786.
[37] Y. Feng, C. Zhang, X. Jiao, Z. Zhou, J. Song, *Energy Storage Mater.* **2020**, *25*, 172.
[38] S.-S. Chi, Q. Wang, B. Han, C. Luo, Y. Jiang, J. Wang, C. Wang, Y. Yu, Y. Deng, *Nano Lett.* **2020**, *20*, 2724.
[39] L. Luo, J. Li, H. Y. Ast, A. Manthiram, *Adv. Mater.* **2019**, *31*, 1904537.
[40] H. Liu, X. Yue, X. Xing, Q. Yan, J. Huang, V. Petrova, H. Zhou, P. Liu, *Energy Storage Mater.* **2019**, *16*, 505.
[41] X.-Y. Yue, W.-W. Wang, Q.-C. Wang, J.-K. Meng, Z.-Q. Zhang, X.-J. Wu, X.-Q. Yang, Y.-N. Zhou, *Energy Storage Mater.* **2018**, *14*, 335.
[42] F. Shen, F. Zhang, Y. Zheng, Z. Fan, Z. Li, Z. Sun, Y. Xuan, B. Zhao, Z. Lin, X. Gui, X. Han, Y. Cheng, C. Niu, *Energy Storage Mater.* **2018**, *13*, 323.

[43] C. Yang, Y. Yao, S. He, H. Xie, E. Hitz, L. Hu, *Adv. Mater.* **2017**, *29*, 1702714.
[44] X. Zhu, H. Cheng, S. Lyu, J. Huang, J. Gu, Y. Guo, Y. Peng, J. Liu, C. Wang, J. Duan, *Adv. Energy Mater.* **2023**, *13*, 2300129.
[45] Z. Cao, H. Chen, Z. Du, J. Gu, Q. Zhu, B. Li, S. Yang, *Adv. Energy Mater.* **2022**, *12*, 2201189.
[46] W. Cao, J. Lu, K. Zhou, G. Sun, J. Zheng, Z. Geng, H. Li, *Nano Energy* **2022**, *95*, 106983.
[47] T. Yu, T. Zhao, N. Zhang, T. Xue, Y. Chen, Y. Ye, F. Wu, R. Chen, *Nano Lett.* **2022**, *23*, 276.
[48] C. Senthil, S. G. Kim, S.-S. Kim, M. G. Hahm, H. Y. Jung, *Small* **2022**, *18*, 2200919.
[49] S. Chang, X. Jin, Q. He, T. Liu, J. Fang, Z. Shen, Z. Li, S. Zhang, M. Dahbi, J. Alami, K. Amine, A.-D. Li, H. Zhang, J. Lu, *Nano Lett.* **2022**, *22*, 263.
[50] J. Zeng, Q. Liu, D. Jia, R. Liu, S. Liu, B. Zheng, Y. Zhu, R. Fu, D. Wu, *Energy Storage Mater.* **2021**, *41*, 697.
[51] M. L. Meyerson, P. E. Papa, A. Heller, C. B. Mullins, *ACS Nano* **2021**, *15*, 29.
[52] Y. Cui, S. Liu, D. Wang, X. Wang, X. Xia, C. Gu, J. Tu, *Adv. Funct. Mater.* **2021**, *31*, 2006380.
[53] B. Han, D. Feng, S. Li, Z. Zhang, Y. Zou, M. Gu, H. Meng, C. Wang, K. Xu, Y. Zhao, H. Zeng, C. Wang, Y. Deng, *Nano Lett.* **2020**, *20*, 4029.
[54] H. Chen, A. Pei, D. Lin, J. Xie, A. Yang, J. Xu, K. Lin, J. Wang, H. Wang, F. Shi, D. Boyle, Y. Cui, *Adv. Energy Mater.* **2019**, *9*, 1900858.
[55] J. Gu, Q. Zhu, Y. Shi, H. Chen, D. Zhang, Z. Du, S. Yang, *ACS Nano* **2020**, *14*, 891.
[56] J. Wang, H. Hu, S. Duan, Q. Xiao, J. Zhang, H. Liu, Q. Kang, L. Jia, J. Yang, W. Xu, H. Fei, S. Cheng, L. Li, M. Liu, H. Lin, Y. Zhang, *Adv. Funct. Mater.* **2022**, *32*, 2110468.
[57] T. Lyu, F. Luo, D. Wang, L. Bu, L. Tao, Z. Zheng, *Adv. Energy Mater.* **2022**, *12*, 2201493.
[58] D. Li, C. Xie, Y. Gao, H. Hu, L. Wang, Z. Zheng, *Adv. Energy Mater.* **2022**, *12*, 2200584.
[59] Z. Xu, L. Xu, Z. Xu, Z. Deng, X. Wang, *Adv. Funct. Mater.* **2021**, *31*, 2102354.
[60] Y.-K. Huang, R. Pan, D. Rehnlund, Z. Wang, L. Nyholm, *Adv. Energy Mater.* **2021**, *11*, 2003674.
[61] K.-H. Chen, A. J. Sanchez, E. Kazyak, A. L. Davis, N. P. Dasgupta, *Adv. Energy Mater.* **2019**, *9*, 1802534.
[62] D. Wang, C. Luan, W. Zhang, X. Liu, L. Sun, Q. Liang, T. Qin, Z. Zhao, Y. Zhou, P. Wang, W. Zheng, *Adv. Energy Mater.* **2018**, *8*, 1800650.
[63] Q. Song, H. Yan, K. Liu, K. Xie, W. Li, W. Gai, G. Chen, H. Li, C. Shen, Q. Fu, S. Zhang, L. Zhang, B. Wei, *Adv. Energy Mater.* **2018**, *8*, 1800564.
[64] L. Sun, M. Li, J. Gu, Y. Li, J. Liu, Y. Li, M. Li, *Chem. Eng. J.* **2023**, *469*, 144014.
[65] H. Liu, E. Wang, Q. Zhang, Y. Ren, X. Guo, L. Wang, G. Li, H. Yu, *Energy Storage Mater.* **2019**, *17*, 253.
[66] T.-S. Wang, Y. Liu, Y.-X. Lu, Y.-S. Hu, L.-Z. Fan, *Energy Storage Mater.* **2018**, *15*, 274.
[67] Y. Cheng, Z. Wang, J. Chen, Y. Chen, X. Ke, D. Wu, Q. Zhang, Y. Zhu, X. Yang, M. Gu, *Angew. Chem., Int. Ed.* **2023**, *62*, 202305723.
[68] J. Cheng, G. Hou, Q. Sun, Q. Chen, D. Li, J. Li, Z. Zeng, K. Li, Q. Yuan, J. Wang, L. Ci, *Sci. China Mater.* **2022**, *65*, 364.
[69] S. Gao, Y. Pan, B. Li, M. A. Rahman, M. Tian, H. Yang, P.-F. Cao, *Adv. Funct. Mater.* **2023**, *33*, 2210543.
[70] T. Zhang, X. Li, X. Miao, R. Sun, J. Li, Z. Zhang, R. Wang, C. Wang, Z. Li, L. Yin, *ACS Appl. Mater. Interfaces* **2022**, *14*, 14264.
[71] C. Mo, L. Quan, W. Zhu, G. Li, X. Wang, Y. Liao, W. Li, *ACS Appl. Energy Mater.* **2022**, *5*, 9118.
[72] D. Yang, J. Li, F. Yang, J. Li, L. He, H. Zhao, L. Wei, Y. Wang, X. Wang, Y. Wei, *Nano Lett.* **2021**, *21*, 7063.
[73] C. Gao, Q. Dong, G. Zhang, H. Fan, H. Li, B. Hong, Y. Lai, *ChemElectroChem* **2019**, *6*, 1134.
[74] P. Liu, J. Zhang, L. Zhong, S. Huang, L. Gong, D. Han, S. Wang, M. Xiao, Y. Meng, *Small* **2021**, *17*, 2102454.
[75] Y. Liu, J. Wu, Y. Yang, *J. Electrochem. Soc.* **2020**, *167*, 160535.
[76] Y. Zhang, Y. Liu, J. Zhou, D. Wang, L. Tan, C. Yi, *Chem. Eng. J.* **2022**, *431*, 134266.
[77] Z. T. Wondimkun, T. T. Beyene, M. A. Weret, N. A. Sahalie, C.-J. Huang, B. Thirumalraj, B. A. Jote, D. Wang, W.-N. Su, C.-H. Wang, G. Brunklaus, M. Winter, B.-J. Hwang, *J. Power Sources* **2020**, *450*, 227589.
[78] R. Pathak, K. Chen, A. Gurung, K. M. Reza, B. Bahrami, J. Pokharel, A. Baniya, W. He, F. Wu, Y. Zhou, K. Xu, Q. Qiao, *Nat. Commun.* **2020**, *11*, 93.
[79] K. Yan, Z. Lu, H.-W. Lee, F. Xiong, P.-C. Hsu, Y. Li, J. Zhao, S. Chu, Y. Cui, *Nat. Energy* **2016**, *1*, 16010.
[80] D. Xu, N. Zhou, A. Wang, Y. Xu, X. Liu, S. Tang, J. Luo, *Adv. Mater.* **2023**, *35*, 2302872.
[81] E. Chason, N. Jadhav, F. Pei, E. Buchovecky, A. Bower, *Prog. Surf. Sci.* **2013**, *88*, 103.
[82] J. W. Shin, E. Chason, *Phys. Rev. Lett.* **2009**, *103*, 056102.
[83] E. Chason, A. Engwall, F. Pei, M. Lafouresse, U. Bertocci, G. Stafford, J. A. Murphy, C. Lenihan, D. N. Buckley, *J. Electrochem. Soc.* **2013**, *160*, D3285.
[84] X. Wang, W. Zeng, L. Hong, W. Xu, H. Yang, F. Wang, H. Duan, M. Tang, H. Jiang, *Nat. Energy* **2018**, *3*, 227.
[85] J. Gu, Y. Tao, H. Chen, Z. Cao, Y. Zhang, Z. Du, Y. Cui, S. Yang, *Adv. Energy Mater.* **2022**, *12*, 2200115.
[86] W. L. Chan, E. Chason, C. Iamsumang, *Nucl. Instrum. Methods Phys. Res., Sect. B* **2007**, *257*, 428.
[87] W. L. Chan, E. Chason, *J. Vac. Sci. Technol. A* **2008**, *26*, 44.
[88] E. Buchovecky, N. Jadhav, A. F. Bower, E. Chason, *J. Electron. Mater.* **2009**, *38*, 2676.
[89] L. Reinbold, N. Jadhav, E. Chason, K. S. Kumar, *J. Mater. Res.* **2009**, *24*, 3583.
[90] E. Chason, *Thin Solid Films* **2012**, *526*, 1.
[91] P. Jagtap, N. Jain, E. Chason, *Scripta Mater.* **2020**, *182*, 43.
[92] G. Abadias, E. Chason, J. Keckes, M. Sebastiani, G. B. Thompson, E. Barthel, G. L. Doll, C. E. Murray, C. H. Stoessel, L. Martinu, *J. Vac. Sci. Technol. A* **2018**, *36*, 020801.
[93] T. Kaub, Z. Rao, E. Chason, G. B. Thompson, *Surf. Coat. 80 [Eighty], Annu. Natl. Tech. Semin., 11th* **2019**, *357*, 939.
[94] E. Chason, A. M. Engwall, Z. Rao, T. Nishimura, *J. Appl. Phys.* **2018**, *123*, 185305.
[95] R. Abermann, *Vacuum* **1990**, *41*, 1279.
[96] E. Chason, P. Jagtap, *J. Appl. Phys.* **2020**, *128*, 145301.
[97] E. Chason, F. Pei, N. Jain, A. Hitt, *J. Electron. Mater.* **2019**, *48*, 17.
[98] R. Hoffman, *Thin Solid Films* **1976**, *34*, 185.
[99] J. A. Thornton, D. Hoffman, *Thin Solid Films* **1989**, *171*, 5.
[100] W. J. Boettinger, C. Johnson, L. A. Bendersky, K.-W. Moon, M. E. Williams, G. R. Stafford, *Acta Mater.* **2005**, *53*, 5033.
[101] Y. He, X. Ren, Y. Xu, M. H. Engelhard, X. Li, J. Xiao, J. Liu, J.-G. Zhang, W. Xu, C. Wang, *Nat. Nanotechnol.* **2019**, *14*, 1042.
[102] L. Zhang, T. Yang, C. Du, Q. Liu, Y. Tang, J. Zhao, B. Wang, T. Chen, Y. Sun, P. Jia, H. Li, L. Geng, J. Chen, H. Ye, Z. Wang, Y. Li, H. Sun, X. Li, Q. Dai, Y. Tang, Q. Peng, T. Shen, S. Zhang, T. Zhu, J. Huang, *Nat. Nanotechnol.* **2020**, *15*, 94.
[103] J. H. Cho, X. Xiao, K. Guo, Y. Liu, H. Gao, B. W. Sheldon, *Energy Storage Mater.* **2020**, *24*, 281.
[104] X. Zhang, Q. Xiang, S. Tang, A. Wang, X. Liu, J. Luo, *Nano Lett.* **2020**, *20*, 2871.
[105] H. Wang, J. Wu, L. Yuan, Z. Li, Y. Huang, *ACS Appl. Mater. Interfaces* **2020**, *12*, 28337.
[106] Q. Liu, Z. Yu, R. Zhou, B. Zhang, *Adv. Funct. Mater.* **2023**, *33*, 2210290.

[107] Y. Liu, X. Yin, X. Shen, P. Zou, X. Qin, C. Yang, Q. Zhang, F. Kang, G. Chen, B. Li, *Adv. Funct. Mater.* **2020**, *30*, 2002522.
[108] Q. Guo, Y. Yu, S. Xia, C. Shen, D. Hu, W. Deng, D. Dong, X. Zhou, G. Z. Chen, Z. Liu, *ACS Appl. Mater. Interfaces* **2022**, *14*, 46043.
[109] J. Chen, X. Qiao, X. Han, J. Zhang, H. Wu, Q. He, Z. Chen, L. Shi, Y. Wang, Y. Xie, *Nano Energy* **2022**, *103*, 107814.
[110] L. Zeng, J. He, C. Yang, D. Luo, H. Yu, H. He, C. Zhang, *Energy Storage Mater.* **2023**, *54*, 469.
[111] Z. Du, C. Wu, Y. Chen, Z. Cao, R. Hu, Y. Zhang, J. Gu, Y. Cui, H. Chen, Y. Shi, J. Shang, B. Li, S. Yang, *Adv. Mater.* **2021**, *33*, 2101473.
[112] Z. Du, C. Wu, Y. Chen, Q. Zhu, Y. Cui, H. Wang, Y. Zhang, X. Chen, J. Shang, B. Li, W. Chen, C. Liu, S. Yang, *Adv. Energy Mater.* **2022**, *12*, 2103228.
[113] G. G. Stoney, C. A. Parsons, *Proc. R. Soc. A* **1909**, *82*, 172.
[114] E. Chason, P. R. Guduru, *J. Appl. Phys.* **2016**, *119*, 191101.
[115] L. B. Freund, S. Suresh, *Thin Film Materials: Stress, Defect Formation and Surface Evolution*, Cambridge University press, Cambridge, **2004**.
[116] S. Mayr, R. Averback, *Phys. Rev. B* **2003**, *68*, 214105.
[117] E. Klokholm, *Rev. Sci. Instrum.* **1969**, *40*, 1054.
[118] A. Rosakis, R. Singh, Y. Tsuji, E. Kolawa, N. Moore Jr, *Thin Solid Films* **1998**, *325*, 42.
[119] J. Floro, E. Chason, S. Lee, R. Twesten, R. Hwang, L. Freund, *J. Electron. Mater.* **1997**, *26*, 969.
[120] C.-H. Chen, E. Chason, P. R. Guduru, *J. Electrochem. Soc.* **2017**, *164*, A574.
[121] T. Valente, C. Bartuli, M. Sebastiani, A. Loreto, *J. Therm. Spray Technol.* **2005**, *14*, 462.
[122] J. Keckes, *J. Appl. Crystallogr.* **2005**, *38*, 311.
[123] J. Keckes, M. Bartosik, R. Daniel, C. Mitterer, G. Maier, W. Ecker, J. Vila-Comamala, C. David, S. Schoeder, M. Burghammer, *Scripta Mater.* **2012**, *67*, 748.

Jianan Gu received his Ph.D. degree in material science at Beihang University in 2020 under the supervision of Prof. Shubin Yang. He is now an associate professor at the North China Electric Power University. His research interests focused on the synthesis of 2D materials and energy storage, including MXenes, Li/Na metal anodes, and Zn anodes.

Yu Shi received his M.S. degree at Northeastern University in 2018 under the supervision of Prof. Yung Joon Jung. He is currently working on his Ph.D. degree at Beihang University under the supervision of Prof. Shubin Yang. His research interests focus on the preparation of MXene-metal composite and their potential applications.

Zhiguo Du obtained his Ph.D. degree at Beihang University in 2020 under the supervision of Prof. Shubin Yang. He is now an associate professor in the School of Materials Science and Engineering at Beihang University. His research interests focus on the preparation of novel 2D materials such as transition-metal chalcogenides and carbides, and their energy storage and conversion applications.

Meicheng Li received his Ph.D. from Harbin Institute of Technology in 2001. During the period from 2004 to 2006, he was a visiting scholar in University of Cambridge. He currently is dean, professor and Ph.D. supervisor of School of New Energy at North China Electric Power University. His research interests focus on solar cell and solar energy utilization technology, lithium/sodium ion battery and energy storage technology, and micro energy and smart energy system.

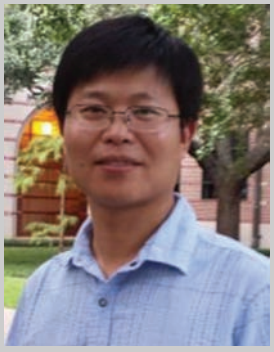

Shubin Yang is a Professor in the Department of Materials Science and Engineering, Beihang University. In 2008, he received his Ph.D. from Beijing University of Chemical Technology. From 2008 to 2014, he worked as a postdoctoral researcher with Prof. K. M¨ullen and P. M. Ajayan at Max Planck Institute for Polymer Research in Germany and Rice University in the United States. From 2017 to 2019, he was selected as "Highly Cited Research" by Clarivate Analytics and "Highly Cited Scholar in China" by Elsevier. His current research interests involve 2D materials for energy storage and conversions.